Tuning the Pyridone Scaffold within a Rhodium-NHC Platform for *gem*-Specific Alkyne Dimerization via a Ligand Assisted Proton Shuttle Mechanism

Belinda Español-Sánchez,[†] María Galiana-Cameo,[†] Asier Urriolabeitia,[‡] Victor Polo,[‡] Vincenzo Passarelli,[†] Jesús J. Pérez-Torrente,[†] Ricardo Castarlenas*[,†]

[†]*Departamento de Química Inorgánica-Instituto de Síntesis Química y Catálisis Homogénea (ISQCH), Universidad de Zaragoza-C.S.I.C., C/Pedro Cerbuna, 12, 50009 Zaragoza, Spain*

[‡]*Departamento de Química Física, Universidad de Zaragoza, C/ Pedro Cerbuna 12, 50009 Zaragoza, Spain*

KEYWORDS Metal-Ligand Cooperation, LAPS, Alkyne Dimerization, N-Heterocyclic Carbene, Hemilability, C-H Activation

ABSTRACT: A series of mononuclear square-planar Rh{κ²*N*,*O*-BHetA}(η²-coe)(NHC) (BHetA = Bis-Heteroatomic Acidato) complexes have been prepared. Modifications on pyridonato BHetA-type ligand architecture include 4-Me, 5-Me, 6-Me, 3-Br, 4-Br, 4-OMe, 5-NO_2 substitution as well as pyrimidonato, succinimidato, and 2-piperidonato catalysts. Two structural isomers have been observed for the complexes, depending on the stereoelectronic properties of the ligand. Structure-activity relationship has been studied for *gem*-specific alkyne dimerization via a cooperative Ligand Assisted Proton Shuttle (LAPS) mechanism. DFT theoretical calculations have revealed a mechanistic pathway involving the hemilabile coordination of the BHetA ligand, CMD deprotonation, π-alkyne protonation and reductive elimination. The increase in oxygen basicity imparted by the substituent in the pyridonato ligand is key, being the 4-methyl derivative the most active catalyst. However, a favored iminol-amide tautomerization precludes an increase of catalytic activity for the more basic saturated piperidonato catalyst.

INTRODUCTION

Over the past two decades, transition-metal-mediated C-H functionalization reactions have been gradually applied in synthetic chemistry to replace C-X or C-M partners in classical cross-coupling processes, as well as in atom economic additions to multiple bonds.[1] Despite the enormous potential of these advanced methodologies, critical challenges remain to be addressed, in particular the typical low reactivity of unactivated C-H bonds and the selectivity issues associated both, with their ubiquitous presence in organic molecules and with regio- and stereo-differentiation in addition reactions. The complexity of C-H activation is reflected in the wide variety of operative mechanisms (Scheme 1).[2] The classical scenario governed by Oxidative Addition (OA), Electrophilic Activation (EA) or σ-bond Metathesis (SBM) has been revisited to include alternative approaches such as Concerted Metallation Deprotonation/Ambiphilic Metal-Ligand Activation (CMD/AMLA),[3] σ-Complex Assisted Metathesis (σ-CAM),[4] Ligand to Ligand Hydrogen Transfer (LLHT)[5] and even radical-mediated[6] or outer-sphere activations.[7] In particular, Metal-Ligand Cooperation (MLC) is undoubtedly responsible for the enhanced catalytic activity of redox-neutral CMD pathways over EA ones, which also allows better control of the selectivity (Scheme 1b).[8] After the initial C-H cleavage by an internal base, subsequent functionalization of the newly formed metal-carbon bond occurs via migratory-insertion (MI) of a multiple bond. The catalytic cycle is then closed by protonolysis (PL), which could also benefit from the advantages of MLC in a Concerted Protonation Demetallation (CPD) framework,[9] which can be considered the microscopic reverse of CMD. On the other hand, the LLHT approach, mainly described for first row transition metals, represents an efficient alternative to the OA route (Scheme 1c). Prior to the final coupling event via reductive elimination (RE), which is common to both oxidative mechanisms, LLHT entails a direct hydrogen transfer between coordinated substrates, in contrast to the two-step pathway through metal-hydride intermediates proposed for OA. Obviously, the reduction of catalytic steps has a critical impact on the catalytic performance in terms of both activity and selectivity.

Scheme 1. Transition-Metal-Mediated C-H Functionalization Approaches

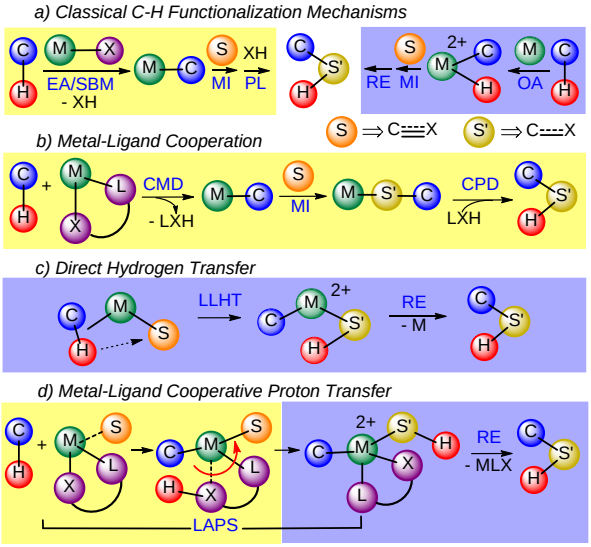

As an alternative, a metal-ligand platform that combines the advantages of both approaches, the MLC of CMD and the rapid proton transfer of LLHT, can be envisaged. Therefore, after the initial MLC-favoured C-H activation of the first substrate, the resulting protonated LXH ligand would not be released from the

metal but would directly protonate the second coordinated substrate. Then, the two metal-organic fragments generated thereof couple through RE (Scheme 1d). The term Ligand Assisted Proton Shuttle (LAPS) has been coined for this type of mechanism.[10] Although originally proposed for intramolecular π-alkyne-vinylidene tautomerization,[11] it has been successfully implemented in catalytic transformations involving alkynes.[12] In particular, we have recently applied the LAPS methodology for *gem*-specific alkyne dimerization promoted by rhodium-*N*-heterocyclic carbene (NHC) platforms (Scheme 2).[13] This atom economic transformation provides straightforward access to conjugated 1,3-enynes, which are key structural subunits in a variety of functional materials and biologically active molecules.[14] Despite the versatile reactivity of alkynes, which makes chemo-, regio- and stereoselectivity a particularly challenging task,[15] efficient dimerization catalysts are widespread across the periodic table, operating under a varied set of mechanisms.[13b,16] Moreover, of particular synthetic difficulty and interest are the formation of head-to-tail *gem*-enynes.[17] In this regard, the dichotomous nature of alkynes enables them to participate in LAPS processes by acting both as the C-H donor through the terminal alkynyl proton and the acceptor partner through the triple bond. In addition, Rh-NHC platforms allow the simultaneous coordination of the two alkyne molecules, thus favoring ligand-mediated proton transfer, which results in an enhancement of the catalytic activity by lowering the key energy barrier by about 5 kcal·mol^{-1} compared to Rh^{III}-hydrometallation or Rh^{I}-carbometallation conventional pathways.[13b]

Scheme 2. Alkyne Dimerization via LAPS Mechanism

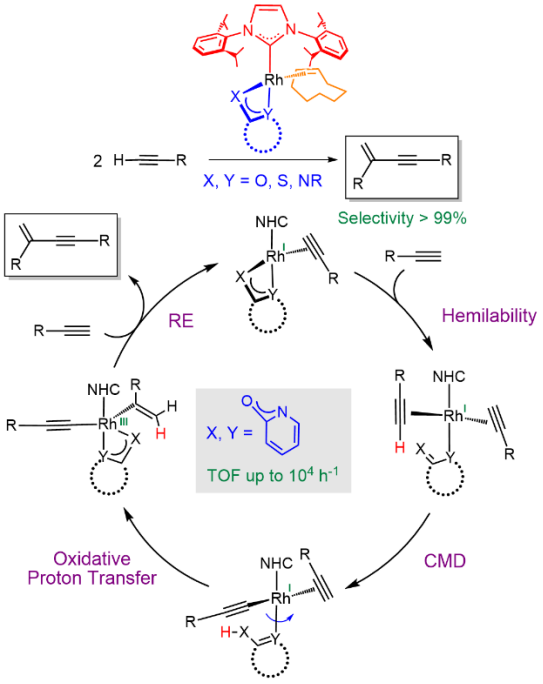

The LAPS pathway also has a significant impact on regioselectivity. In general, the type of insertion of the triple bond into metal-hydride or metal-alkynyl intermediates (1,2 or 2,1) determines the formation of head-to-head or head-to-tail dimers.[15] However, a precise control over this step is rather complex, since it depends on the metal center and the stereoelectronic properties of ancillary ligands. Alternatively for the LAPS approach, protonation of a π-coordinated alkyne is faster than insertion and it is highly favored over the terminal position for electron-rich or neutral alkynes,[18] therefore resulting in specific formation of Markovnikov-type *gem*-enynes (Scheme 3).

Scheme 3. Regioselectivity-Determining Step in Alkyne Dimerization

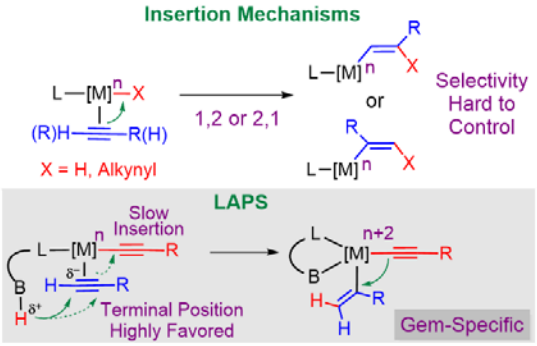

Critical requirements for an efficient proton shuttle ligand would be: *i*) an adequate basicity to deprotonate C-H bonds, *ii*) the ability of the conjugated acid to subsequently protonate another substrate and *iii*) tight coordination to the metallic center throughout the whole process. We envisaged that κ^2-chelate 1,3-Bis-Hetereoatomic Acidato ligands (BHetA), such as carboxylato, thioacidato, amidinato, or amidato species might fulfill these prerequisites.[13a] However only the *N*,*O*-BHetA species gave satisfactory catalytic results. Thus, thioacidato ligands do not seem to be basic enough, while amidinato species would be less efficient in the protonation step. The low activity of carboxylato counterparts is somewhat surprising, since they are typically the ligand of choice in base-mediated C-H activation reactions via CMD-insertion-protonolysis events due to their ability to deprotonate and protonate efficiently (Scheme 1b). Most likely, the lability of the protonated form would prevent it from acting as an MLC proton shuttle. Among the *N*,*O*-BHetA ligands, the Rh-NHC-pyridonato catalyst was the most active. It showed astonishing levels of catalytic activity, reaching TOFs values up to 10^4 h^{-1}.[13b] In addition to a versatile compendium of basicity and coordination properties, 2-pyridonato architectures can also be finely tuned due to their modular building principle.[19]

One of the main research aims in our laboratories is the development of key catalytic transformations through the judicious design of catalysts based on mechanistic understanding and structure-activity relationship. In this context, the fine-tuning of the catalyst topology to optimize the catalytic outcomes is somewhat analogous to the adjustment of the homogeneity of the magnetic field in a NMR experiment, hence the term "*Shim Chemistry*" is coined. We have already applied this idea in the development of successive generations of *gem*-selective alkyne hydrothiolation catalysts.[20] In this way, herein, we are continuing the endeavor in the upgrading of alkyne dimerization Rh-NHC catalysts.[13,15,21] Now, we disclose structural modifications in the pyridone-like architecture to study how steric and electronic effects affect alkyne dimerization catalytic activity.

RESULTS AND DISCUSSION

Preparation of Rh-BHetA Catalysts. The dinuclear precursor [Rh(μ-Cl)(η^2-coe)(IPr)]$_2$[22] (**1**) {IPr = 1,3-bis-(2,6-diisopropylphenyl)imidazolin-2-carbene; coe = cyclooctene} reacts with an in-situ prepared THF solution of BHetA ligands to yield derivatives Rh{κ^2*N*,*O*-(OCN-R)}(η^2-coe)(IPr) (**3-13**) (Scheme 4). The analogous complex bearing the parent pyridone (Opy) Rh{κ^2*N*,*O*-(Opy)}(η^2-coe)(IPr) (**2**) has been previously described by us.[13b] The new complexes were obtained as yellow

solids, except the orange nitro-derivative **8**, in 63-73% yields due to slight solubility in *n*-hexane used as the precipitating solvent. Typically, a thermodynamic mixture of two isomers is observed due to the orientation of the nitrogen and oxygen atoms of the BHetA moiety with regard to the IPr or coe ligands. Theoretical[23] and experimental[13,20,24] studies have shown the preference of the nitrogen atom of pyridine-type ligands to coordinate trans to a NHC in d^8 square-planar complexes, thus, this configuration is predominantly observed (isomer **a**). However, functionalization of the α-position to the nitrogen atom in 6-methyl pyridonato (**5**) or succinimidato derivatives (**11-12**), significantly increase the amount of the isomer **b** due to steric factors (*vide infra*).[20c]

Scheme 4. Preparation of Rh-IPr-BHetA Catalysts

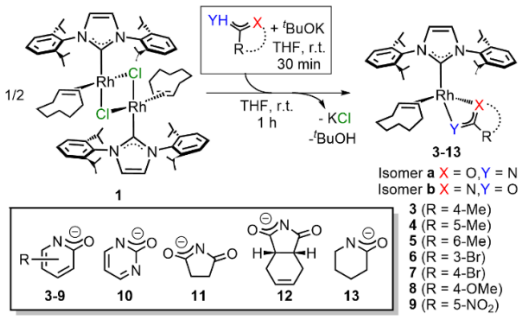

The solid-state structure of complexes **5**, **7**, **10**, **11**, and **13** were elucidated by X-ray diffraction analysis (Figure 1). All of them show a distorted square planar environment at the metal center with a cis arrangement of the NHC and coe ligands, and the two remaining coordination sites are occupied by the nitrogen and oxygen atoms of the BHetA moiety. In all cases isomer **a** is observed, even for the succinimidato derivative **11**, in which species **b** is the major isomer in solution (**a**:**b** 38:62). Thus, the oxygen atom of the BHetA moiety lies trans to the coe ligand (CT-Rh-O 168˚, av.) whereas the nitrogen atom occupies the remaining coordination site virtually trans to NHC (C1-Rh-N 159˚, av.). The small bite angle of the BHetA moiety (O-Rh-N 62˚, av.) brings up a severely distorted coordination with respect to the rhodium-nitrogen bond affording yaw angles at nitrogen in the range 28.8-34.9˚. As for the NHC ligand, it lies almost perpendicular to the coordination plane rendering angles between the C1-N2-C3-C4-N5 plane and the coordination plane of about 72˚ (av.). Indeed, the NHC ligand shows a slight deviation from the ideal arrangement with respect to the rhodium-carbon bond (see pitch and yaw angles in Figure 1). Particularly, the steric impact due to the introduction of a 6-methyl substituent in **5** is reflected in a distortion in the coordination of the BHetA ligand by a lengthening of the R-N30 bond {2.2811(17) *vs* 2.15 Å av.}, a reduction of the C1-Rh-N30 angle {154.58(7)˚ *vs* 160˚ av.} and an enlargement of the CT-Rh-O36 angle {173.75(4)˚ *vs* 167˚ av}. Moreover, it is worth a mention that, the κ^2*N*,*O* coordination mode of the BHetA ligand is quite exceptional in **10**, **11** and **13**, since, to the best of our knowledge, only one example of each of them, namely Ni(κ^2*N*,*O*-pyrimidonato)$_2$,[25a] MoH(κ^2*N*,*O*-succinimidato)(dppe)$_2$,[25b] and Ni(*p*-Tol)(κ^2*N*,*O*-piperidonato)(IPr),[25c] have been described so far.

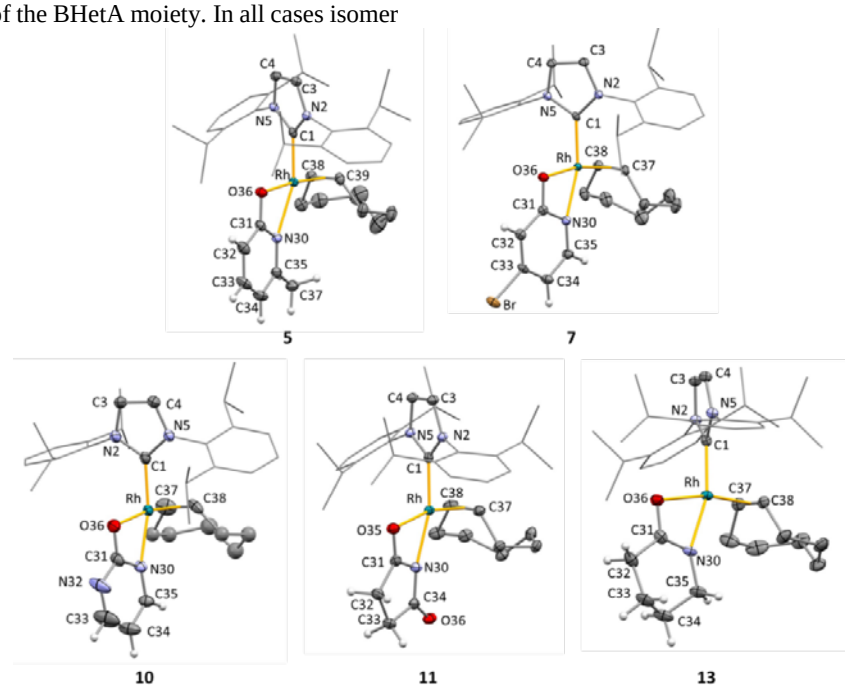

Figure 1. ORTEP view of crystal structures of **5**, **7**, **10**, **11**, and **13**. Most hydrogen atoms are omitted for clarity. Ellipsoids are at 50% probability. Selected bond lengths (Å) and angles (˚) are: **5**, C1-Rh 1.934(2), O36-Rh 2.0931(15), N30-Rh 2.2811(17), Rh-CT 1.97439(15), O36-Rh-N30 61.57(6), C1-Rh-N30 154.58(7), CT-Rh-O36 173.75(4); **7**, C1-Rh 1.9570(15), N30-Rh 2.1527(13), O36-Rh 2.1358(11), Rh-CT 1.97109(13), O36-Rh-N30 62.83(5), C1-Rh-N30 158.13(6), CT-Rh-O36 167.97(3); **10**, C1-Rh 1.957(3), N30-Rh 2.131(3), O36-Rh 2.135(2), Rh-CT 1.9680(2), N30-Rh-O36 62.73(9), C1-Rh-N30 160.14(12), CT-Rh-O36 168.12(7); **11**, C1-Rh 1.9469(10), N30-Rh 2.1585(9), O35-Rh 2.2213(9), Rh-CT 1.96028(17), N30-Rh-O35 61.33(3), C1-Rh-N30 162.80(4), CT-Rh-O35 164.76(2); **13**, C1-Rh 1.954(2), N30-Rh 2.1471(19), O36-Rh 2.1358(17), Rh-CT 1.9696(2), O36-Rh-N30 62.07(7), C1-Rh-N30 160.49(9), CT-Rh-O36 167.05(5). Pitch and yaw angles (˚): **5**, 9.7, 1.9, NHC, 4.2, 34.3, BHetA; **7**, 10.7, 1.0, NHC, 8.5, 30.7, BHetA; **10**, 2.6, 1.0, NHC, 2.4, 30.5 BHetA; **11**, 5.2, 0.8, NHC, 1.0, 34.9, BHetA; **13**, 5.6, 1.4, NHC; 0.2, 28.8, BHetA. CT, centroid of the C=C bond of the coe ligand.

The NMR spectroscopic data are in agreement with the mononuclear square-planar structure observed in the solid state for **5**, **7**, **10**, **11**, and **13**. Spectral assignment were made by combination of ^{1}H, ^{13}C{^{1}H}-APT, ^{1}H-^{1}H COSY, ^{1}H-^{1}H NOESY, ^{1}H-^{13}C HSQC and ^{1}H-^{13}C HMBC NMR experiments recorded in C_6D_6. Due to solubility issues, NMR data for **7** were collected in CD_2Cl_2, while toluene-d_8 at 243 K was used to obtain an acceptable resolution of the spectra of the succinimidato-type complexes **11** and **12**. The spectra of **3**-**13** showed the characteristic resonances of IPr, coe, and 1,3-BHetA ligands, including typical rhodium-carbon couplings around 60 and 16 Hz for IPr ($C_{carbenic}$) and coe ($C_{olefinic}$), respectively, whereas values of 2-3 Hz were found for the Rh-OCN carbon atom of BHetA ligands in **3**-**10**, which is consistent with a κ^2-coordination mode. The ^{1}H-^{15}N long range HMQC 2D-NMR spectra show cross-peaks around δ_N 200 and 192 ppm for nitrogen atoms of pyridonato ligands and IPr, respectively. Moreover, the uncoordinated nitrogen atom of the pyrimidonato moiety in **10** resonates at 261.0 ppm, whereas that of valerolactamato ligand in **13** is observed at 143.4 ppm (see SI).

Particularly informative about the structure and behavior of Rh-IPr complexes in solution are the signals corresponding to CH-isopropyl protons on the carbene wings, which appear as septuplets in the ^{1}H NMR spectra. The intrinsic four signals could converge into two or one depending on symmetry elements as well as a rotational process of the carbene ligand around the Rh-C axis.[23a] In the present case, this behavior is useful to discriminate between isomers **a** and **b** (see Figure 2 for **11**). Thus, the ^{1}H NMR spectrum at 243 K (a) displays one septuplet at 3.06 ppm for isomer **11a**, as a result of a symmetry plane containing the BHetA ligand and bisecting IPr and coe, as well as the fast rotation of the carbene ligand. However, two septuplets at 3.98 and 2.03 ppm are observed for isomer **11b**, since rotation of the carbene is hindered by the carbonyl group of the succinimidato ligand. Both isomers are in a dynamic equilibrium as demonstrated by the presence of exchange peaks in the ^{1}H-^{1}H NOESY NMR experiment even at 243 K. In agreement to this, only one set of signals is observed at the high temperature fast limit (Figure 2b). The activation parameters for the isomerization process obtained from the corresponding Eyring analysis were $\Delta H^{\neq} = 21.3 \pm 0.8$ kcal·mol^{-1} and $\Delta S^{\neq} = 29.9 \pm 2.1$ e.u.

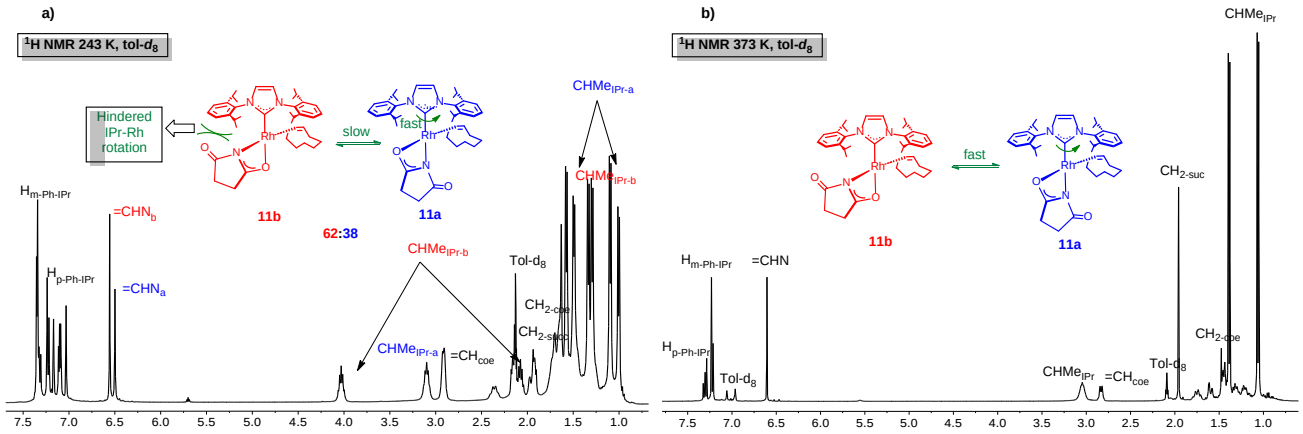

Figure 2. ^{1}H NMR spectra of **11a,b** under low-temperature slow regime (a) and high-temperature fast limit (b).

In the case of pyridonato complexes, the introduction of a methyl group *ortho* to the nitrogen atom in **5** has a significant effect on the increment of the ratio of the **b** isomer (**a**:**b**, 49:51), pointing to a steric origin (Figure 3). Although somewhat counterintuitive, the hindrance of a coe ligand is *higher* than that of the bulky IPr.[20c] Actually, the anisotropy of the latter allows the methyl group of the pyridonato to accommodate between the bis-isopropylphenyl wingtips of the carbene, which is reflected by a NOE interaction between the methyl group and the imidazolinyl protons within **5b**. In contrast, the pseudo-spherical cyclooctene does not allow for this steric relief. In fact, only the thermodynamically more stable isomer **14a** was observed when the olefin in **5** was replaced by a linear 3-hexyne.

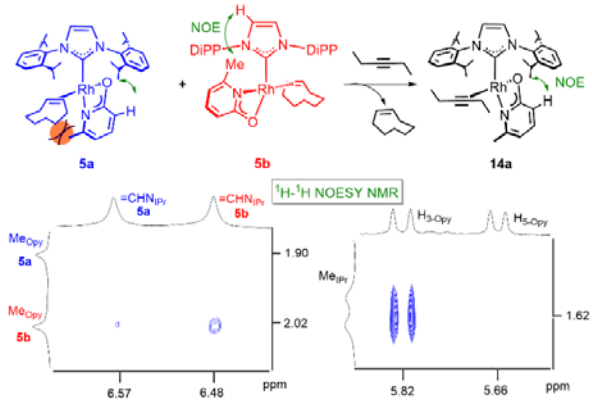

Figure 3. Selected region of the ^{1}H-^{1}H NOESY NMR spectra of the coe derivatives **5a**:**5b** (left) and the η^2-3-hexyne complex **14a** (right).

Catalytic Alkyne Dimerization. The catalytic activity of the Rh-NHC-BHetA complexes **3**-**13** in alkyne dimerization was

evaluated. As previously observed for complex **2**, the dimerization rate of phenylacetylene was very fast, so 1-hexyne was initially used as a benchmark substrate (Figure 4). Catalytic reactions were performed in C_6D_6 solutions at room temperature using a 2 mol% catalyst loading. Conversion of 1-hexyne to the enyne 7-methylidene-undec-5-yne was monitored by ^{1}H NMR spectroscopy using mesitylene as an internal standard. Subtle modifications on the heterocyclic core of the BHetA ligand result in an adjustment of electronic and steric influence over critical steps of catalytic process (see Scheme 2). Thus, modified-pyridonato derivatives **3-4**, **6-9** chemo- and regioselectively convert the alkyne into the head-to-tail enyne in less than 5 min with a 2 mol% catalyst loading at room temperature. However, the introduction of a methyl group in *ortho* position of the nitrogen atom in **5** drastically decreases the catalytic activity. The steric hindrance likely hampers the coordination of protonated BHetA ligand after the CMD step, thereby inhibiting the proton transfer. Moreover, the introduction of a second carbonyl group in succinimidato derivatives **12-13** also gives very poor results. In this case, the electronic effect could be masked by a steric hindrance similar to that observed for **5**. Thus, the subsequent modifications to the pyridone ring were selected for their low steric influence. Firstly, with the aim of decreasing the barrier of the deprotonation step which proved to be rate limiting,[13b] the more basic piperidonato precursor **13** was evaluated. However, a slight decrease in catalytic activity was observed (*vide infra* theoretical section for discussion). Indeed, the more acidic 2-pyrimidonato catalyst **10** also decreases the catalytic activity.

In order to better decipher the effect of pyridone substitution on catalytic activity, dimerization of other less reactive alkynes was evaluated. Interestingly, significant differences in activity between the catalysts have been observed in the dimerization of methyl propargyl ether (Figure 5a). The electron-withdrawing groups, such as -NO_2 and -Br, reduced the catalytic activity with regard to parent pyridonato catalyst, whereas a higher rate was observed with electron-donating substituents such as methyl. Moreover, dimerization of the rather unreactive mesitylacetylene shows that 4-methylpyridonato catalyst **3** is the most active catalyst of this series (Figure 5b).

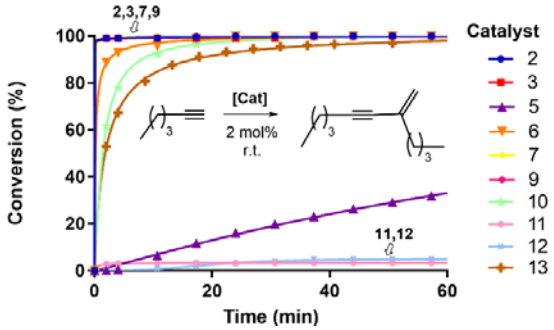

Figure 4. Reaction profile for the dimerization of 1-hexyne using 2 mol% catalyst loading at room temperature.

The electronic effect of a substituent at a pyridine-2-olato heterocycle, the aromatic tautomeric form of 2-pyridonato, would be an interplay of that exerted over the two functionalities. The influence over the nitrogen atom will affect the hemilabile behavior, whereas that over the oxygen atom is related to basicity. In this context, a methoxy substituent is quite helpful since its electronic effect is reversed when it is in *meta* or *para* positions. Thus, the Hammett analysis fits better when considering the effect over the oxygen atom, implying that basicity is more relevant to the catalytic outcome than hemilabilty (Figure 5c, see Figure S1 in the SI for Hammett plot analysis considering the effect over the nitrogen atom).

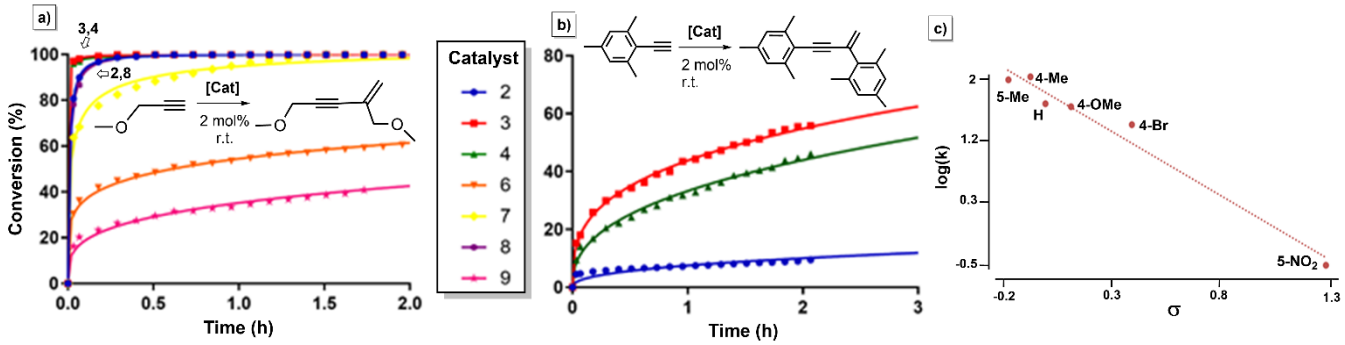

Figure 5. Reaction profile for dimerization of methyl propargyl ether (a) and mesitylacetylene (b) using different pyridone-functionalized catalysts (2 mol%). (c) Hammett plot analysis considering the effect over the oxygen atom in pyridine-2-olato tautomer.

Once complex **3** was revealed as the most active catalyst, low loading experiments were carried out using phenylacetylene as substrate (Figure 6). Total conversion and selectivity towards 1,3-diphenyl-but-3-en-1-yne was observed in less than 30 min with 0.1 mol% catalyst loading. Moreover, even at a reduced catalyst loading to 0.05 mol%, **3** is still efficient and shows a roughly double $TOF_{1/2}$ value when compared to the parent pyridonato complex **2**.[13b]

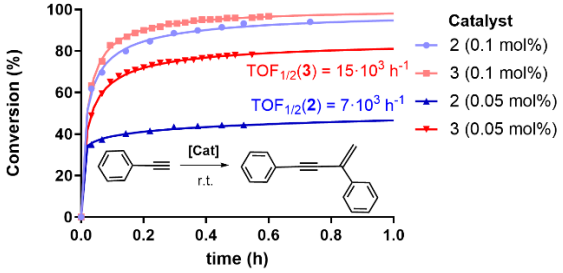

Figure 6. Comparison of the catalytic activity of **2** and **3** in the dimerization of phenylacetylene at room temperature.

Theoretical calculations on the influence of the κ²*O,N*-BHetA ligand on the reaction mechanism. A DFT study has been performed in order to understand the electronic effects that different κ²*N,O*-BHetA ligands induce on the catalyst performance. Four derivatives have been considered: **2** (2-pyridonato), **3** (4-methyl-2-pyridonato), **10** (2-pyrimidonato), and **13** (2-piperidonato). According to the proposed mechanism (Scheme 2), the basicity at the oxygen atom of the BHetA ligand might play a key role on the catalytic activity, because rate-determining step is CMD of the alkyne by the anionic ligand.[11b] Thus, gas phase basicity (GB) values for the four ligands have been determined at the same computational level. GB values of anionic species are defined as the Gibbs energy change associated with the protonation reaction in the gas phase (Eq. 1). Hence, the oxygen basicity shows de following trend: pyrimidonato (227.7 kcal·mol^{-1}) < pyridonato (233.6 kcal·mol^{-1}) ~ 4-Me-pyridonato (234.7 kcal·mol^{-1}) < piperidonato (242.1 kcal·mol^{-1}).

$$B^- + H^+ \rightarrow BH \quad (1)$$

The DFT energetic profile for the alkyne dimerization of phenylacetylene catalyzed by the four BHetA derivatives is shown in Figure 7. The starting point is the Rh{κ²*O,N*-BHetA}(η²-alkyne)(IPr) species (**A**) and the relative values of Δ*G* in kcal·mol^{-1} are presented. The more relevant energetic barriers are associated with the ligand hemilability, CMD and protonation, being determined by **TSAB**, **TSBC**, and **TSCD**, respectively. According to the energetic span model,[26] the TDTS (TOF Determining Transition State) for the unsaturated BHetA ligands in **2**, **3** and **10** is that of the CMD step (**TSBC**), whereas the TDI (TOF Determining Intermediate) is the starting point **A**. In agreement with the superior catalytic performance observed experimentally for the 4-methylpyridonato catalyst **3**, it displays the lower energetic span within unsaturated heterocyclic catalysts. A different situation is observed for the more basic valerolactamato catalyst **13**. Athough all significant transition states are located *below* those calculated for its unsaturated analogs, no increase in catalytic activity was observed experimentally (*vide supra*). The rationale for this intriguing fact arises from the iminol-amide tautomerization within intermediate **C** to **C'**. The stabilization is more pronounced for the saturated species **13**. Therefore, the -7.4 kcal·mol^{-1} value of **C'** makes it the TDI for **13**, hence, the energetic span increases up to 18.9 kcal·mol^{-1}.

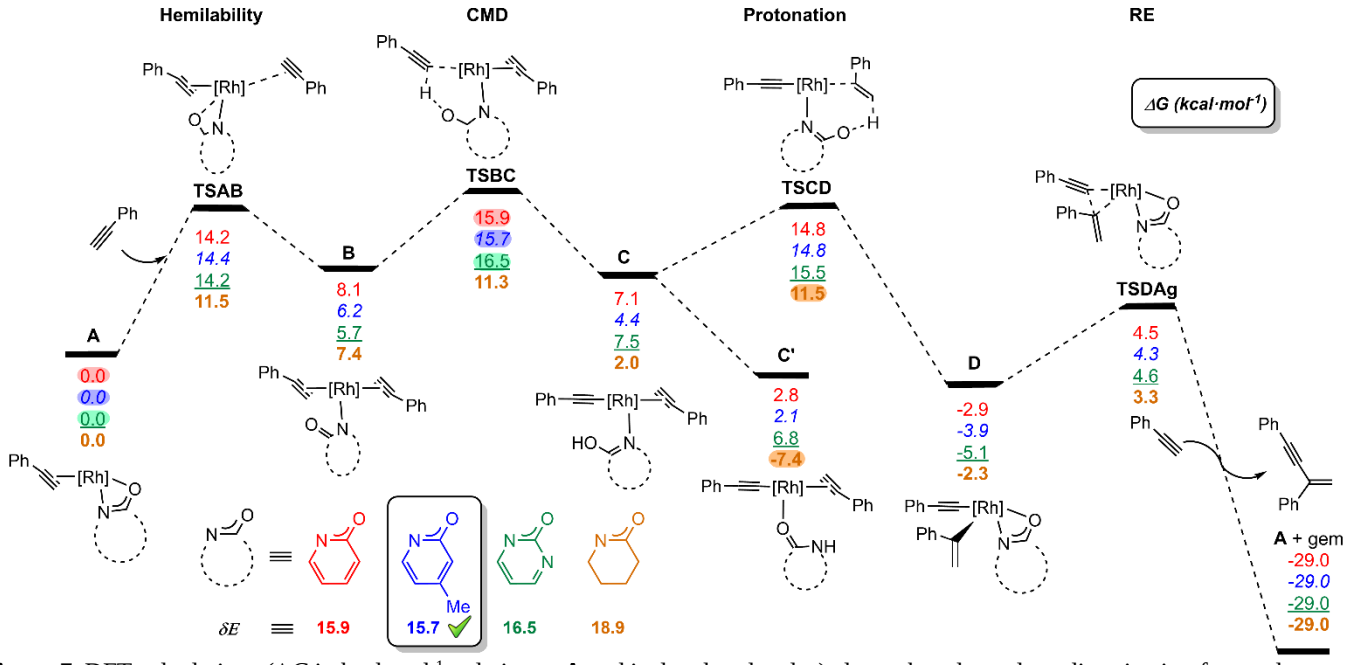

Figure 7. DFT calculations (Δ*G* in kcal·mol^{-1}, relative to **A** and isolated molecules) along phenylacetylene dimerization for catalysts **2** (red), **3** (blue, italic), **10** (green, underline), and **13** (brown, bold).

CONCLUSION

A series of mononuclear square-planar Rh{κ²*N,O*-BHetA}(η²-coe)(IPr) complexes have been prepared as efficient catalysts for *gem*-specific alkyne dimerization via a cooperative LAPS mechanism. A fine-tuning of the pyridone-like structure in the framework of *Shim Chemistry* has been carried out in order to study their structure-activity relationship. Depending on the orientation of the BHetA ligand two structural isomers in dynamic equilibrium are observed. The configuration with the nitrogen atom disposed trans-to-IPr is preferred, except for those ligands with α-to-nitrogen substitution in which the enhanced steric hindrance of the pseudo-spherical coe with respect to the anisotropic bulky IPr is significant, and produces a reversal preferred orientation of the κ²*N,O*-ligand.

Computational studies reveal an operative pathway involving hemilabile decoordination of the BHetA ligand, deprotonation of the first alkyne via a CMD process, subsequent protonation of a second π-coordinated alkyne, and final alkynyl-alkenyl reductive elimination. Substitution at the *ortho* position of the nitrogen atom leads to the decoordination of the ligand after CMD step which is detrimental for catalytic activity. DTF calculations show that hemilabilty, CMD, and protonation steps have similar energetic barriers, with CMD being the TDTS for unsaturated BHetA ligands, whereas protonation is for the more basic saturated piperidonato species. Catalytic activity increases in parallel with the oxygen basicity of the BHetA ligand as a consequence of the substituents at unsaturated heterocycles. Thus, the 4-methylpyridonato catalyst is the most active of the series with a TOF approximately twice of that of the parent

pyridonato catalyst. However, the increased basicity of the saturated valerolactamato BHetA ligand does not lead to an improvement of catalytic activity. The rationale for this fact steams from a favored lactim-lactam tautomerization within protonated intermediate species, resulting in an increase of the energetic barrier for the subsequent protonation step. The underlying principles revealed herein pave the way to further applying the LAPS methodology to related C−C and C−heteroatom bond forming catalytic reactions via C-H activation.

EXPERIMENTAL SECTION

General Considerations: All reactions were carried out with rigorous exclusion of air and moisture using Schlenk-tube techniques and a dry box when necessary. Reagents were purchased from commercial sources and used as received except for alkynes which were dried over molecular sieves. Particularly, phenylacetylene was first dried over molecular sieves and then distilled and stored over anhydrous $CaCl_2$. Organic solvents were obtained oxygen- and water-free from a Solvent Purification System (Innovative Technologies). Deuterated solvents C_6D_6 and toluene-d_8 were dried with sodium, while calcium hydride was used for drying CD_2Cl_2. The organometallic precursor [Rh(μ-Cl)(η²-coe)(IPr)]$_2$ (**1**)[22] was prepared as previously described in the literature.[22] NMR chemical shifts (expressed in parts per million) are referenced to residual solvent peaks (^{1}H and ^{13}C) and NH_3 (^{15}N). Coupling constants, *J*, are given in hertz (Hz). Spectral assignments were achieved by combination of ^{1}H, ^{13}C{^{1}H}-APT, ^{1}H-^{1}H COSY, and ^{1}H-^{13}C HSQC and HMBC experiments. The 2D ^{1}H-^{15}N HMQC long range experiments were recorded with a $J_{N\text{-}H}$ = 10 or 4 Hz. Attenuated total reflection infrared spectra (ATR-IR) of solid samples were recorded on a PerkinElmer Spectrum 100 FT-IR spectrometer. C, H, and N analyses were carried out in a Perkin-Elmer 2400 CHNS/O analyzer. High-resolution electrospray ionization mass spectra (HRMS-ESI) were recorded using a Bruker MicroToF-Q equipped with an API-ESI source and a Q-ToF mass analyzer, which leads to a maximum error in the measurement of 5 ppm, using sodium formate as a reference.

Preparation of Rh{κ²*N,O*-(4-Me-Opy)}(η²-coe)(IPr) (3). A mixture of 4-methyl-2-pyridone (53 mg, 0.48 mmol) and KO^{t}Bu (53 mg, 0.47 mmol) in 15 mL of THF was stirred for 30 min at r. t. Then, a solution of the dinuclear complex [Rh(μ²-Cl)(η²-coe)$_2$(IPr)]$_2$ **1** (300 mg, 0.24 mmol) in 10 mL of THF was cannulated and the mixture was stirred for 1 h at r.t. After removal of the solvent, the residue was dissolved in toluene (10 mL) and it was filtered through celite. Then, the filtrate was evaporated to dryness. Addition of hexane at -20 °C induced the precipitation of a yellow solid, which was washed with cold hexane (3 x 2 mL) and dried in vacuo. Yield: 240 mg (71%). Anal. calcd for $C_{41}H_{56}N_3ORh$: C, 69.38; H, 7.95; N, 5.92. Found: C, 69.35; H, 8.03; N, 5.83. IR (cm^{-1}, ATR): 1608 ν(OCN$_{sym}$), 1465 ν(OCN$_{asym}$). ^{1}H NMR (400 MHz, C_6D_6, 298 K): δ 7.3–7.1 (7H, H$_{6\text{-}Opy}$, H$_{Ph\text{-}IPr}$), 6.54 (s, 2H, =CHN), 5.98 (dd, $J_{H\text{-}H}$ = 1.7, 0.8, 1H, H$_{3\text{-}Opy}$), 5.75 (dd, $J_{H\text{-}H}$ = 5.6, 1.7, 1H, H$_{5\text{-}Opy}$), 3.21 (sept, $J_{H\text{-}H}$ = 6.8, 4H, C<u>H</u>Me$_{IPr}$), 2.77 (m, 2H, =CH$_{coe}$), 1.9–1.2 (12H, CH$_{2\text{-}coe}$), 1.78 (s, 3H, Me$_{Opy}$), 1.57 and 1.08 (both d, $J_{H\text{-}H}$ = 6.8, 24H, Me$_{IPr}$). ^{13}C{^{1}H}-APT NMR (100.5 MHz, C_6D_6, 298 K): δ 186.0 (d, $J_{C\text{-}Rh}$ = 60.9, Rh-C$_{IPr}$), 181.9 (d, $J_{C\text{-}Rh}$ = 3.2, C$_{2\text{-}Opy}$), 149.7 (s, C$_{4\text{-}Opy}$), 147.1 (s, C$_{q\text{-}IPr}$), 144.0 (s, C$_{6\text{-}Opy}$), 137.3 (s, C$_q$N), 129.8 and 123.9 (both s, CH$_{Ph\text{-}IPr}$), 124.2 (s, =CHN), 110.7 (d, $J_{C\text{-}Rh}$ = 1.2, C$_{3\text{-}Opy}$), 110.2 (s, C$_{5\text{-}Opy}$), 57.0 (d, $J_{C\text{-}Rh}$ = 16.4, =CH$_{coe}$), 30.5 (d, $J_{C\text{-}Rh}$ = 1.6, CH$_{2\text{-}coe}$), 30.3 (d, $J_{C\text{-}Rh}$ = 1.1, CH$_{2\text{-}coe}$), 29.9 (s, <u>C</u>HMe$_{IPr}$), 27.2 (s, CH$_{2\text{-}coe}$), 26.6 and 23.2 (both s, Me$_{IPr}$), 21.3 (s, Me$_{Opy}$). ^{1}H-^{15}N HMQC (long range) NMR (40.5 MHz, C_6D_6, 298 K): δ 201.4 (N$_{Opy}$), 191.8 (N$_{IPr}$).

Preparation of Rh{κ²*N,O*-(5-Me-Opy)}(η²-coe)(IPr) (4). This complex was prepared as described for **3** starting from 5-methyl-2-pyridone (35 mg, 0.32 mmol), KO^{t}Bu (35 mg, 0.31 mmol) and **1** (200 mg, 0.16 mmol). Yield: 164 mg (73%), yellow solid. Anal. calcd for $C_{41}H_{56}N_3ORh$: C, 69.38; H, 7.95; N, 5.92. Found: C, 69.33; H, 8.32; N, 5.82. IR (cm^{-1}, ATR): 1603 ν(OCN$_{sym}$), 1478 ν(OCN$_{asym}$). ^{1}H NMR (400 MHz, C_6D_6, 298 K): δ 7.3–7.1 (7H, H$_{6\text{-}Opy}$, H$_{Ph\text{-}IPr}$), 6.81 (dd, $J_{H\text{-}H}$ = 8.4, 2.3, 1H, H$_{4\text{-}Opy}$), 6.56 (s, 2H, =CHN), 6.05 (d, $J_{H\text{-}H}$ = 8.4, 1H, H$_{3\text{-}Opy}$), 3.22 (sept, $J_{H\text{-}H}$ = 6.8, 4H, C<u>H</u>Me$_{IPr}$), 2.78 (m, 2H, =CH$_{coe}$), 1.9–1.2 (12H, CH$_{2\text{-}coe}$), 1.67 (s, 3H, Me$_{Opy}$), 1.57 and 1.09 (both d, $J_{H\text{-}H}$ = 6.8, 24H, Me$_{IPr}$). ^{13}C{^{1}H}-APT NMR (100.5 MHz, C_6D_6, 298 K): δ 186.0 (d, $J_{C\text{-}Rh}$ = 61.5, Rh-C$_{IPr}$), 180.2 (d, $J_{C\text{-}Rh}$ = 3.1, C$_{2\text{-}Opy}$), 147.2 (s, C$_{q\text{-}IPr}$), 143.8 (s, C$_{6\text{-}Opy}$), 140.1 (s, C$_{4\text{-}Opy}$), 137.3 (s, C$_q$N), 129.8 and 123.9 (both s, CH$_{Ph\text{-}IPr}$), 124.2 (s, =CHN), 116.5 (s, C$_{5\text{-}Opy}$), 110.2 (d, $J_{C\text{-}Rh}$ = 1.2, C$_{3\text{-}Opy}$), 57.0 (d, $J_{C\text{-}Rh}$ = 16.5, =CH$_{coe}$), 30.5 (d, $J_{C\text{-}Rh}$ = 1.6, CH$_{2\text{-}coe}$), 30.3 (d, $J_{C\text{-}Rh}$ = 1.1, CH$_{2\text{-}coe}$), 29.1 (s, <u>C</u>HMe$_{IPr}$), 27.2 (s, CH$_{2\text{-}coe}$), 26.6 and 23.2 (both s, Me$_{IPr}$), 17.6 (s, Me$_{Opy}$). ^{1}H-^{15}N HMQC (long range) NMR (40.5 MHz, C_6D_6, 298 K): δ 206.7 (N$_{Opy}$), 192.1 (N$_{IPr}$).

Preparation of Rh{κ²*N,O*-(6-Me-Opy)}(η²-coe)(IPr) (5a,b). This complex was prepared as described for **3** starting from 6-methyl-2-pyridone (35 mg, 0.32 mmol), KO^{t}Bu (35 mg, 0.31 mmol) and **1** (200 mg, 0.16 mmol). Yield: 152 mg (68%), yellow solid. Anal. calcd for $C_{41}H_{56}N_3ORh$: C, 69.38; H, 7.95; N, 5.92. Found: C, 69.25; H, 8.28; N, 5.97. IR (cm^{-1}, ATR): 1594 ν(OCN$_{sym}$), 1462 ν(OCN$_{asym}$). NMR data evidenced the presence of two isomers in dynamic equilibrium, **5a** and **5b** (49:51 at 298K). Data for **5a:** ^{1}H NMR (400 MHz, C_6D_6, 298 K): δ 7.3-7.0 (6H, H$_{Ph\text{-}IPr}$), 7.03 (t, $J_{H\text{-}H}$ = 7.8, 1H, H$_{4\text{-}Opy}$), 6.57 (s, 2H, =CHN), 6.10 (d, $J_{H\text{-}H}$ = 8.5, 1H, H$_{3\text{-}Opy}$), 5.81 (d, $J_{H\text{-}H}$ = 7.2, 1H, H$_{5\text{-}Opy}$), 3.21 (sept, $J_{H\text{-}H}$ = 6.8, 4H, C<u>H</u>Me$_{IPr}$), 2.67 (m, 2H, =CH$_{coe}$), 1.90 (s, 3H, Me$_{Opy}$), 1.8–1.2 (12H, CH$_{2\text{-}coe}$), 1.54 and 1.07 (both d, $J_{H\text{-}H}$ = 6.8, 24H, Me$_{IPr}$).^{13}C{^{1}H}-APT NMR (100.5 MHz, C_6D_6, 298 K): δ 182.9 (d, $J_{C\text{-}Rh}$ = 67.6, Rh-C$_{IPr}$), 181.1 (d, $J_{C\text{-}Rh}$ = 2.5, C$_{2\text{-}Opy}$), 154.7 (s, C$_{6\text{-}Opy}$), 146.9 (s, C$_{q\text{-}IPr}$), 138.3 (s, C$_{4\text{-}Opy}$), 136.8 (s, C$_q$N), 129.5 and 123.5 (both s, CH$_{Ph\text{-}IPr}$), 124.1 (s, =CHN), 109.3 (s, C$_{5\text{-}Opy}$), 107.6 (s, C$_{3\text{-}Opy}$), 56.1 (d, $J_{C\text{-}Rh}$ = 16.4, =CH$_{coe}$), 30.2, 29.8, and 26.8 (all s, CH$_{2\text{-}coe}$), 28.7 (s, <u>C</u>HMe$_{IPr}$), 26.3 and 22.9 (all s, Me$_{IPr}$), 23.8 (s, Me$_{Opy}$). ^{1}H-^{15}N NMR HMQC (long range) (40.5 MHz, C_6D_6, 298 K): δ 215.8 (N$_{Opy}$), 192.4 (N$_{IPr}$). Data for **5b:** δ 7.3-7.0 (6H, H$_{Ph\text{-}IPr}$), 6.99 (t, $J_{H\text{-}H}$ = 7.8, 1H, H$_{4\text{-}Opy}$), 6.48 (s, 2H, =CHN), 6.04 (d, $J_{H\text{-}H}$ = 8.5, 1H, H$_{3\text{-}Opy}$), 6.01 (d, $J_{H.H}$ = 7.2, 1H, H$_{5\text{-}Opy}$), 4.06 (sept, $J_{H\text{-}H}$ = 6.8, 2H, C<u>H</u>Me$_{IPr}$), 2.88 (m, 2H, =CH$_{coe}$), 2.02 (s, 3H, Me$_{Opy}$), 2.00 (sept, $J_{H\text{-}H}$ = 6.8, 2H, C<u>H</u>Me$_{IPr}$), 1.8–1.2 (12H, CH$_{2\text{-}coe}$), 1.33, 1.25, 1.13, and 0.99 (all d, $J_{H\text{-}H}$ = 6.8, 24H, Me$_{IPr}$). ^{13}C{^{1}H}-APT NMR (100.5 MHz, C_6D_6, 298 K): 192.4 (d, $J_{C\text{-}Rh}$ = 57.5, Rh-C$_{IPr}$), 180.2 (d, $J_{C\text{-}Rh}$ = 2.7, C$_{2\text{-}Opy}$), 151.0 (s, C$_{6\text{-}Opy}$), 147.2 and 146.1 (both s, C$_{q\text{-}IPr}$), 138.2 (s, C$_{4\text{-}Opy}$), 136.8 (s, C$_q$N), 129.4, 124.5, and 123.4 (all s, CH$_{Ph\text{-}IPr}$), 124.1 (s, =CHN), 109.1 (s, C$_{3\text{-}Opy}$), 106.6 (s, C$_{5\text{-}Opy}$), 60.5 (d, $J_{C\text{-}Rh}$ = 16.4, =CH$_{coe}$), 30.1, 27.8, and 26.6 (all s, CH$_{2\text{-}coe}$), 28.8 and 28.5 (both s, <u>C</u>HMe$_{IPr}$), 26.3, 25.8, 23.3, and 22.1 (all s, Me$_{IPr}$), 23.1 (s, Me$_{Opy}$). ^{1}H-^{15}N HMQC (long range) NMR (40.5 MHz, C_6D_6, 298 K): δ 210.2 (N$_{Opy}$), 192.5 (N$_{IPr}$).

Preparation of Rh{κ²*N,O*-(3-Br-Opy)}(η²-coe)(IPr) (6a,b). This complex was prepared as described for **3** starting from 3-bromo-2-pyridone (55 mg, 0.32 mmol), KO^{t}Bu (35 mg, 0.31 mmol) and **1** (200 mg, 0.16 mmol). Yield: 155 mg (63%), yellow solid. Anal. calcd for $C_{40}H_{53}N_3BrORh$: C, 62.02; H, 6.90; N, 5.42. Found: C, 61.85; H, 6.75; N, 5.51. IR (cm^{-1}, ATR): 1586 ν(OCN$_{sym}$), 1459 ν(OCN$_{asym}$). NMR data evidenced the presence of two isomers in dynamic equilibrium, **6a** and **6b** (95:5 at 298 K). Data for **6a**: ^{1}H NMR (400 MHz, C_6D_6, 298 K): δ 7.3-7.0 (6H, H$_{Ph\text{-}IPr}$), 7.29 (dd, $J_{H\text{-}H}$ = 7.6, 5.4, 1H, H$_{4\text{-}Opy}$), 7.13 (d, $J_{H\text{-}H}$ = 5.4, 1H, H$_{6\text{-}OPy}$), 6.55 (s, 2H, =CHN), 5.55 (dd, $J_{H\text{-}H}$ = 7.6, 5.4, 1H, H$_{5\text{-}Opy}$), 3.15 (sept, $J_{H\text{-}H}$ = 6.8, 4H, C<u>H</u>Me$_{IPr}$), 2.82 (m, 2H, =CH$_{coe}$), 1.9–1.1 (12H, CH$_{2\text{-}coe}$), 1.57 and 1.07 (both d, $J_{H\text{-}H}$ = 6.8, 24H, Me$_{IPr}$).^{13}C{^{1}H}-APT NMR (100.5 MHz, C_6D_6, 298 K): δ 184.8 (d, $J_{C\text{-}Rh}$ = 60.8, Rh-C$_{IPr}$), 176.5 (d, $J_{C\text{-}Rh}$ = 3.5, C$_{2\text{-}Opy}$), 147.0 (s, C$_{q\text{-}IPr}$), 143.6 (s, C$_{6\text{-}Opy}$), 141.1 (s, C$_{4\text{-}Opy}$), 137.0 (s, C$_q$N), 130.0 and 124.0 (both s, CH$_{Ph\text{-}IPr}$), 124.5 (s, =CHN), 109.1 (s, C$_{5\text{-}Opy}$), 106.2 (d, $J_{C\text{-}Rh}$ = 1.8, C$_{3\text{-}Opy}$), 57.1 (d, $J_{C\text{-}Rh}$ = 16.8, =CH$_{coe}$), 30.3, 30.2, and 27.1 (all s, CH$_{2\text{-}coe}$), 29.1 (s, <u>C</u>HMe$_{IPr}$), 26.7 and 23.3 (all s, Me$_{IPr}$). ^{1}H-^{15}N HMQC (long range) NMR (40.5 MHz, C_6D_6, 298 K): δ 211.2 (N$_{Opy}$), 192.3 (N$_{IPr}$). Data for **6b**: ^{1}H NMR (400 MHz, C_6D_6, 298 K): δ 7.34 (dd, $J_{H\text{-}H}$ = 7.6, 5.4, 1H, H$_{4\text{-}Opy}$), 7.02 (d, $J_{H\text{-}H}$ = 5.4, 1H, H$_{6\text{-}Opy}$), 6.47 (s, 2H, =CHN), 5.79 (dd, J$_{H.H}$ = 7.6, 5.4, 1H, H$_{5\text{-}Opy}$).

Preparation of Rh{κ²*N,O*-(4-Br-Opy)}(η²-coe)(IPr) (7a,b). This complex was prepared as described for **3** starting from 4-bromo-2-pyridone (55 mg, 0.32 mmol), KO^{t}Bu (35 mg, 0.31 mmol) and **1** (200 mg, 0.16 mmol). Yield: 179 mg (73%), yellow solid. Anal. calcd for $C_{40}H_{53}N_3BrORh$: C, 62.02; H, 6.90; N, 5.42. Found: C, 61.67; H, 7.13; N, 5.48. IR (cm^{-1}, ATR): 1573 ν(OCN$_{sym}$), 1465 ν(OCN$_{asym}$). NMR data evidenced the presence of two isomers in dynamic equilibrium, **7a** and **7b** (86:14 at 298 K). Data for **7a**: ^{1}H NMR (400 MHz, CD_2Cl_2,

298 K): δ 7.5-7.3 (6H, $H_{Ph\text{-}IPr}$), 7.02 (d, $J_{H\text{-}H}$ = 5.9, 1H, $H_{6\text{-}Opy}$), 6.97 (s, 2H, =CHN), 6.14 (dd, $J_{H\text{-}H}$ = 5.9, 2.0, 1H, $H_{5\text{-}Opy}$), 5.96 (d, $J_{H\text{-}H}$ = 2.0, 1H, $H_{3\text{-}Opy}$), 2.93 (sept, $J_{H\text{-}H}$ = 6.8, 4H, C<u>H</u>Me_{IPr}), 2.60 (m, 2H, =CH_{coe}), 1.5–1.1 (12H, $CH_{2\text{-}coe}$), 1.41 and 1.11 (both d, $J_{H\text{-}H}$ = 6.8, 24H, Me_{IPr}).$^{13}C\{^1H\}$-APT NMR (100.5 MHz, CD_2Cl_2, 298 K): δ 182.6 (d, $J_{C\text{-}Rh}$ = 61.6, Rh-C_{IPr}), 180.2 (d, $J_{C\text{-}Rh}$ = 2.5, $C_{2\text{-}Opy}$), 146.9 (s, $C_{q\text{-}IPr}$), 145.3. (s, $C_{6\text{-}Opy}$), 136.7 (s, C_qN), 133.2 (s, $C_{4\text{-}Opy}$), 130.0 and 124.2 (both s, $CH_{Ph\text{-}IPr}$), 125.0 (s, =CHN), 113.4 (s, $C_{3\text{-}Opy}$), 112.0 (s, $C_{5\text{-}Opy}$), 58.1 (d, $J_{C\text{-}Rh}$ = 16.3, =CH_{coe}), 30.3, 30.2, and 27.1 (all s, $CH_{2\text{-}coe}$), 29.4 (s, <u>C</u>HMe_{IPr}), 26.7 and 23.2 (all s, Me_{IPr}). $^1H\text{-}^{15}N$ HMQC (long range) NMR (40.5 MHz, CD_2Cl_2, 298 K): δ 205.8 (N_{Opy}), 192.0 (N_{IPr}). Data for **7b**: ^1H NMR (400 MHz, CD_2Cl_2, 298 K): δ 7.5-7.3 (6H, $H_{Ph\text{-}IPr}$), 7.15 (d, $J_{H\text{-}H}$ = 5.9, 1H, $H_{6\text{-}Opy}$), 7.01 (s, 2H, =CHN), 6.36 (dd, $J_{H\text{-}H}$ = 5.9, 2.0, 1H, $H_{5\text{-}Opy}$), 6.03 (d, $J_{H.H}$ = 2.0, 1H, $H_{3\text{-}Opy}$), 2.87 (m, 2H, =CH_{coe}), 2.76 (sept, $J_{H\text{-}H}$ = 6.8, 4H, C<u>H</u>Me_{IPr}), 1.5–1.0 (12H, $CH_{2\text{-}coe}$), 1.20 and 1.12 (both d, $J_{H\text{-}H}$ = 6.8, 24H, Me_{IPr}).$^{13}C\{^1H\}$-APT NMR (100.5 MHz, CD_2Cl_2, 298 K): δ 184.5 (d, $J_{C\text{-}Rh}$ = 61.6, Rh-C_{IPr}), 178.1 (d, $J_{C\text{-}Rh}$ = 2.5, $C_{2\text{-}Opy}$), 146.4 (s, $C_{q\text{-}IPr}$), 145.1 (s, $C_{6\text{-}Opy}$), 136.5 (s, C_qN), 133.4 (s, $C_{4\text{-}Opy}$), 130.2 and 124.3 (both s, $CH_{Ph\text{-}IPr}$), 125.4 (s, =CHN), 115.1 (s, $C_{3\text{-}Opy}$), 111.9 (s, $C_{5\text{-}Opy}$), 62.6 (d, $J_{C\text{-}Rh}$ = 16.3, =CH_{coe}), 30.3, 30.2, and 28.3 (all s, $CH_{2\text{-}coe}$), 29.4 (s, <u>C</u>HMe_{IPr}), 26.6 and 22.8 (all s, Me_{IPr}). $^1H\text{-}^{15}N$ NMR (long range) NMR (40.5 MHz, CD_2Cl_2, 298 K): δ 200.7 (N_{Opy}), 192.2 (N_{IPr}).

Preparation of Rh{κ²*N,O*-(4-OMe-Opy)}(η²-coe)(IPr) (8a,b). This complex was prepared as described for **3** starting from 4-methoxy-2-pyridone (40 mg, 0.32 mmol), KO^{t}Bu (35 mg, 0.31 mmol) and **1** (200 mg, 0.16 mmol). Yield: 175 mg (75%), yellow solid. Anal. calcd for $C_{41}H_{56}N_3O_2Rh.H_2O$: C, 66.20; H, 7.86; N, 5.65. Found: C, 66.09; H, 7.97; N, 5.70. IR (cm^{-1}, ATR): 1601 ν(OCN_{sym}), 1465 ν(OCN_{asym}). NMR data evidenced the presence of two isomers in dynamic equilibrium, **8a** and **8b** (92:8 at 298 K). Data for **8a**: ^1H NMR (400 MHz, C_6D_6, 298 K): δ 7.3-7.1 (6H, $H_{Ph\text{-}IPr}$), 7.14 (d, $J_{H\text{-}H}$ = 6.3, 1H, $H_{6\text{-}Opy}$), 6.56 (s, 2H, =CHN), 5.73 (dd, $J_{H\text{-}H}$ = 6.3, 2.4, 1H, $H_{5\text{-}Opy}$), 5.63 (d, $J_{H\text{-}H}$ = 2.4, 1H, $H_{3\text{-}Opy}$), 3.22 (sept, $J_{H\text{-}H}$ = 6.8, 4H, C<u>H</u>Me_{IPr}), 3.14 (s, 3H, OMe), 2.76 (m, 2H, =CH_{coe}), 1.5–1.1 (12H, $CH_{2\text{-}coe}$), 1.58 and 1.10 (both d, $J_{H\text{-}H}$ = 6.8, 24H, Me_{IPr}).$^{13}C\{^1H\}$-APT NMR (100.5 MHz, C_6D_6, 298 K): δ 186.0 (d, $J_{C\text{-}Rh}$ = 60.8, Rh-C_{IPr}), 183.2 (d, $J_{C\text{-}Rh}$ = 2.1, $C_{2\text{-}Opy}$), 168.8 (s, $C_{4\text{-}Opy}$), 147.1 (s, $C_{q\text{-}IPr}$), 145.0 (s, $C_{6\text{-}Opy}$), 137.3 (s, C_qN), 129.9 and 124.0 (both s, $CH_{Ph\text{-}IPr}$), 124.2 (s, =CHN), 99.1 (s, $C_{5\text{-}Opy}$), 92.8 (s, $C_{3\text{-}Opy}$), 56.7 (d, $J_{C\text{-}Rh}$ = 16.8, =CH_{coe}), 54.2 (s, OMe), 30.5, 30.3, and 27.2 (all s, $CH_{2\text{-}coe}$), 29.2 (s, <u>C</u>HMe_{IPr}), 26.6 and 23.2 (all s, Me_{IPr}). $^1H\text{-}^{15}N$ HMQC (long range) NMR (40.5 MHz, C_6D_6, 298 K): δ 192.2 (N_{IPr}) 191.8 (N_{Opy}). Data for **8b**: ^1H NMR (400 MHz, C_6D_6, 298 K): δ 7.3-7.1 (6H, $H_{Ph\text{-}IPr}$), 6.50 (s, 2H, =CHN), 6.01 (dd, $J_{H\text{-}H}$ = 6.3, 2.6, 1H, $H_{5\text{-}Opy}$), 5.55 (d, $J_{H\text{-}H}$ = 2.6, 1H, $H_{3\text{-}Opy}$), 3.08 (s, 3H, OMe). $^{13}C\{^1H\}$-APT NMR (100.5 MHz, C_6D_6, 298 K): δ 168.0 (s, $C_{4\text{-}Opy}$), 146.7 (s, $C_{q\text{-}IPr}$), 144.6 (s, $C_{6\text{-}Opy}$), 99.6 (s, $C_{5\text{-}Opy}$), 93.5 (s, $C_{3\text{-}Opy}$), 61.3 (d, $J_{C\text{-}Rh}$ = 15.9, =CH_{coe}).

Preparation of Rh{κ²*N,O*-(5-NO₂-Opy)}(η²-coe)(IPr) (9a,b). This complex was prepared as described for **3** starting from 5-nitro-2-pyridone (44 mg, 0.32 mmol), KO^{t}Bu (35mg, 0.31 mmol) and **1** (200 mg, 0.16 mmol). Yield: 158 mg (68%), orange solid. Anal. calcd for $C_{40}H_{53}N_4O_3Rh.H_2O$: C, 63.32; H, 7.31; N, 7.38. Found: C, 63.31; H, 7.29; N, 7.44. IR (cm^{-1}, ATR): 1595 ν(OCN_{sym}), 1458 ν(OCN_{asym}). NMR data evidenced the presence of an equilibrium mixture of two isomers, **9a** and **9b** (91:9 at 298 K).Data for **9a:** ^1H NMR (400 MHz, C_6D_6, 298 K): δ 8.42 (d, $J_{H\text{-}H}$ = 2.9, 1H, $H_{6\text{-}Opy}$), 7.69 (dd, $J_{H\text{-}H}$ = 9.0, 2.9, 1H, $H_{4\text{-}Opy}$), 7.3-7.1 (6H, $H_{Ph\text{-}IPr}$), 6.52 (s, 2H, =CHN), 5.61 (d, $J_{H.H}$ = 9.0, 1H, $H_{3\text{-}Opy}$), 3.03 (sept, $J_{H\text{-}H}$ = 6.8, 4H, C<u>H</u>Me_{IPr}), 2.84 (m, 2H, =CH_{coe}), 1.9–1.1 (12H, $CH_{2\text{-}coe}$), 1.47 and 1.05 (both d, $J_{H\text{-}H}$ = 6.8, 24H, Me_{IPr}).$^{13}C\{^1H\}$-APT NMR (100.5 MHz, C_6D_6, 298 K): δ 183.0 (d, $J_{C\text{-}Rh}$ = 61.4, Rh-C_{IPr}), 182.3 (d, $J_{C\text{-}Rh}$ = 2.9, $C_{2\text{-}Opy}$), 146.9 (s, $C_{q\text{-}IPr}$), 144.2 (s, $C_{6\text{-}Opy}$), 136.8 (s, C_qN), 134.6 (s, $C_{4\text{-}Opy}$), 133.4 (s, $C_{5\text{-}Opy}$), 130.2 and 124.0 (both s, $CH_{Ph\text{-}IPr}$), 124.7 (s, =CHN), 109.7 (s, $C_{3\text{-}Opy}$), 58.6 (d, $J_{C\text{-}Rh}$ = 16.8, =CH_{coe}), 30.1, 30.0, and 26.9 (all s, $CH_{2\text{-}coe}$), 29.1 (s, <u>C</u>HMe_{IPr}), 26.6 and 23.1 (both s, Me_{IPr}). $^1H\text{-}^{15}N$ HMQC (long range) NMR (40.5 MHz, C_6D_6, 298 K): δ 366.7 (NO_2), 210.5 (N_{Opy}), 192.9 (N_{IPr}). Data for **9b:** ^1H NMR (400 MHz, C_6D_6, 298 K): δ 8.72 (d, $J_{H\text{-}H}$ = 2.9, 1H, $H_{6\text{-}OPy}$), 7.78 (dd, $J_{H\text{-}H}$ = 9.0, 2.9, 1H, $H_{4\text{-}OPy}$),7.3-7.1 (6H, $H_{Ph\text{-}IPr}$), 6.47 (s, 2H, =CHN), 5.65 (d, $J_{H.H}$ = 9.0, 1H, $H_{3\text{-}OPy}$), 3.16 (m, 2H, =CH_{coe}), 2.84 (sept, $J_{H\text{-}H}$ = 6.8, 4H, C<u>H</u>Me_{IPr}), 1.9–1.1 (12H, $CH_{2\text{-}coe}$), 1.21 and 1.05 (both d, $J_{H\text{-}H}$ = 6.8, 24H, Me_{IPr}). $^{13}C\{^1H\}$-APT NMR (100.5 MHz, C_6D_6, 298 K): δ 146.5 (s, $C_{q\text{-}IPr}$), 144.2 (s, $C_{6\text{-}Opy}$), 136.8 (s, C_qN), 134.6 (s, $C_{4\text{-}Opy}$), 130.2 and 124.0 (both s, $CH_{Ph\text{-}IPr}$), 125.0 (s, =CHN), 111.7 (s, $C_{3\text{-}Opy}$), 63.8 (d, $J_{C\text{-}Rh}$ = 16.8, =CH_{coe}), 30.1, 30.0, and 27.0 (all s, $CH_{2\text{-}coe}$), 29.2 (s, <u>C</u>HMe_{IPr}), 26.3 and 22.5 (both s, Me_{IPr}).

Preparation of Rh{κ²*N,O*-($C_4H_3N_2O$)}(η²-coe)(IPr) (10). This complex was prepared as described for **3** starting from pyrimidin-2-one (31 mg, 0.32 mmol), KO^{t}Bu (35 mg, 0.31 mmol) and **1** (200 mg, 0.16 mmol). Yield: 147 mg (66%), yellow solid. Anal. calcd for $C_{39}H_{53}N_4O_1Rh$: C, 67.23; H, 7.67; N, 8.04. Found: C, 67.49; H, 7.86; N, 7.78. IR (cm^{-1}, ATR): 1575 ν(OCN_{sym}), 1544 ν(OCN_{sym}), 1482 ν(OCN_{asym}), 1461 ν(OCN_{asym}). ^1H NMR (400 MHz, C_6D_6, 298 K): δ 8.07 (dd, $J_{H\text{-}H}$ = 4.7, 2.8, 1H, $H_{4\text{-}Opym}$), 7.27 (dd, $J_{H\text{-}H}$ = 4.7, 2.8, 1H, $H_{6\text{-}Opym}$), 7.3-7.2 (6H, $H_{Ph\text{-}IPr}$), 6.55 (s, 2H, =CHN), 5.53 (dd, $J_{H.H}$ = 4.8, 4.8, 1H, $H_{5\text{-}Opym}$), 3.17 (sept, $J_{H\text{-}H}$ = 6.8, 4H, C<u>H</u>Me_{IPr}), 2.84 (m, 2H, =CH_{coe}), 1.9–1.1 (12H, $CH_{2\text{-}coe}$), 1.58 and 1.07 (both d, $J_{H\text{-}H}$ = 6.8, 24H, Me_{IPr}). $^{13}C\{^1H\}$-APT NMR (100.5 MHz, C_6D_6, 298 K): δ 184.4 (d, $J_{C\text{-}Rh}$ = 62.3, Rh-C_{IPr}), 177.06 (d, $J_{C\text{-}Rh}$ = 3.7, $C_{2\text{-}Opym}$), 160.7 (s, $C_{4\text{-}Opym}$), 154.0 (s, $C_{6\text{-}Opym}$), 147.2 (s, $C_{q\text{-}IPr}$), 137.0 (s, C_qN), 107.6 (s, $C_{5\text{-}Opym}$), 130.0 and 124.0 (both s, $CH_{Ph\text{-}IPr}$), 124.5 (s, =CHN), 57.7 (d, $J_{C\text{-}Rh}$ = 17.3, =CH_{coe}), 30.5, 30.3, and 27.2 (all s, $CH_{2\text{-}coe}$), 29.0 (s, <u>C</u>HMe_{IPr}), 26.6 and 23.3 (both s, Me_{IPr}). $^1H\text{-}^{15}N$ HMQC (long range) NMR (40.5 MHz, C_6D_6, 298 K): δ 261.0 ($N_{3\text{-}Opym}$), 199.9 ($N_{1\text{-}Opym}$), 192.4 (N_{IPr}).

Preparation of Rh{κ²*N,O*-($C_4H_4NO_2$)}(η²-coe)(IPr) (11a,b). This complex was prepared as described for **3** starting from pirrolidine-2,5-dione (31 mg, 0.32 mmol), KO^{t}Bu (35 mg, 0.31 mmol) and **1** (200 mg, 0.16 mmol). Yield: 143 mg (65%), yellow solid. Anal. calcd for $C_{39}H_{54}N_3O_2Rh$: C, 66.94; H, 7,78; N, 6.00. Found: C, 66.65; H, 7.77; N, 5.86. IR (cm^{-1}, ATR): 1699 ν(C=O), 1564 ν(OCN_{sym}), 1465 ν(OCN_{asym}). NMR data evidenced the presence of two isomers in dynamic equilibrium, **11a** and **11b** (38:62 at 243 K). Data for **11a**: ^1H NMR (400.1 MHz, toluene-d_8, 243 K): δ 7.4-7.0 (m, 6H, $H_{Ph\text{-}IPr}$), 6.46 (s, 2H, =CHN), 3.06 (sept, $J_{H\text{-}H}$ = 6.8, 4H, C<u>H</u>Me_{IPr}), 2.87 (m, 2H, =CH_{coe}), 2.12 and 1.88 (both m, 4H, $CH_{2\text{-}suc}$), 2.0-0.9 (m, 12H, $CH_{2\text{-}coe}$), 1.53 and 0.96 (both d, $J_{H\text{-}H}$ = 6.8, 24H, Me_{IPr}). $^{13}C\{^1H\}$-APT NMR (100.6 MHz, toluene-d_8, 243 K): δ 201.4 (s, Rh-NC=O), 184.5 (d, $J_{C\text{-}Rh}$ = 1.7, Rh-OCN), 182.8 (d, $J_{C\text{-}Rh}$ = 60.7, Rh-C_{IPr}), 146.4 (s, $C_{q\text{-}IPr}$), 136.7 (s, C_qN), 129.9 and 124.5 (both s, $CH_{m\text{-}Ph\text{-}IPr}$), 124.4 (s, =CHN), 123.1 (s, $CH_{p\text{-}Ph\text{-}IPr}$), 58.9 (d, $J_{C\text{-}Rh}$ = 18.0, =CH_{coe}), 31.4, 30.5, and 26.7 (all s, $CH_{2\text{-}coe}$), 30.0 (s, $CH_{2\text{-}suc}$), 29.0 (s, <u>C</u>HMe_{IPr}), 26.3 and 22.8 (both s, Me_{IPr}). Data for **11b**: ^1H NMR (400.1 MHz, toluene-d$_8$, 243 K): δ 7.4-7.0 (m, 6H, $H_{Ph\text{-}IPr}$), 6.52 (s, 2H, =CHN), 3.98 and 2.03 (both sept, $J_{H\text{-}H}$ = 6.8, 4H, C<u>H</u>Me_{IPr}), 2.87 (m, 2H, =CH_{coe}), 2.12 and 1.88 (both m, 4H, $CH_{2\text{-}suc}$), 2.0-0.9 (m, 12H, $CH_{2\text{-}coe}$), 1.45, 1.29, 1.25, and 1.06 (all d, $J_{H\text{-}H}$ = 6.8, 24H, Me_{IPr}). $^{13}C\{^1H\}$-APT NMR (100.6 MHz, toluene-d_8, 243 K): δ 201.4 (s, Rh-NC=O), 184.5 (d, $J_{C\text{-}Rh}$ = 1.7, Rh-OCN), 181.7 (d, $J_{C\text{-}Rh}$ = 66.7, Rh-C_{IPr}), 148.0 and 145.8 (both s, $C_{q\text{-}IPr}$), 136.8 (s, C_qN), 129.9, 129.8, 124.5, and 123.9 (all s, $CH_{m\text{-}Ph\text{-}IPr}$), 124.4 (s, =CHN), 123.1 (s, $CH_{p\text{-}Ph\text{-}IPr}$), 60.0 (d, $J_{C\text{-}Rh}$ = 15.7, =CH_{coe}), 30.6, 29.8, and 28.0 (all s, $CH_{2\text{-}coe}$), 30.8 and 27.0 (both s, $CH_{2\text{-}suc}$), 28.7 and 28.6 (both s, <u>C</u>HMe_{IPr}), 26.8, 26.5, 22.6, and 22.0 (all s, Me_{IPr}).

Preparation of Rh{κ²*N,O*-($C_8H_8NO_2$)}(η²-coe)(IPr) (12a,b). This complex was prepared as described for **3** starting from cis-1,2,3,6-tetrahydrophthalimide (40 mg, 0.32 mmol), KO^{t}Bu (35 mg, 0.31 mmol) and **1** (200 mg, 0.16 mmol). Yield: 165 mg (69%), yellow solid. Anal. calcd for $C_{43}H_{58}N_3O_2Rh$: C, 68.69; H, 7,78; N, 5.59. Found: C, 68.38; H, 7.86; N, 5.72. IR (cm^{-1}, ATR): 1701 ν(C=O), 1552 ν(OCN_{sym}), 1466 ν(OCN_{asym}). NMR data evidenced the presence of two isomers in dynamic equilibrium, **12a** and **12b** (47:53 at 243 K). Data for **12a**: ^1H NMR (400.1 MHz, toluene-d_8, 243 K): δ 7.4-7.0 (m, 6H, $H_{Ph\text{-}IPr}$), 6.47 (s, 2H, =CHN), 5.70 (br, 2H, HC=CH_{Pht}), 3.11 (sept, $J_{H\text{-}H}$ = 6.8, 4H, C<u>H</u>Me_{IPr}), 2.85 (m, 2H, =CH_{coe}), 2.36 (m, 4H, $CH_{2\text{-}pht}$), 2.12 (m, 2H, CH_{pht}), 2.3-0.9 (36H, $CH_{2\text{-}coe,}$ Me_{IPr}). $^{13}C\{^1H\}$-APT NMR (100.6 MHz, toluene-d_8, 243 K): δ 203.0 (s, Rh-NC=O), 186.8 (s, Rh-OCN), 182.4 (d, $J_{C\text{-}Rh}$ = 61.0, Rh-C_{IPr}), 146.2 (s, $C_{q\text{-}IPr}$), 136.5 (s, C_qN), 129-122 ($CH_{Ph\text{-}IPr}$), 127.5 (s, HC=CH_{pht}), 123.7 (s, =CHN), 59.0 (d, $J_{C\text{-}Rh}$ = 17.0, =CH_{coe}), 41.4 (s, CH_{pht}), 30.6, 26.8, and 23.2 (all s, $CH_{2\text{-}coe}$), 29.0 (s, <u>C</u>HMe_{IPr}), 26.1 and 22.8 (both s, Me_{IPr}), 22.3 (s, $CH_{2\text{-}pht}$). Data for **12b**: ^1H NMR (400.1 MHz, toluene-d$_8$, 243 K): δ 7.4-7.0 (m, 6H, $H_{Ph\text{-}IPr}$),

6.54 and 6.52 (both br, 2H, =CHN), 5.84 and 5.60 (both br, 2H, HC=CH$_{pht}$), 4.09, 3.95, 2.09 and 2.07 (all sept, J_{H-H} = 6.8, 4H, CHMe$_{IPr}$), 2.94 (m, 2H, =CH$_{coe}$), 2.72, 2.39, 2.33, and 1.91 (m, 4H, CH$_{2-pht}$), 2.51 and 2.40 (both m, 2H, CH$_{pht}$), 2.3-0.9 (36H, CH$_{2-coe,}$ Me$_{IPr}$). ^{13}C{^{1}H}-APT NMR (100.6 MHz, toluene-d_8, 243 K): δ 203.0 (s, Rh-NC=O), 186.8 (s, Rh-OCN), 181.5 (d, J_{C-Rh} = 66.1, Rh-C$_{IPr}$), 148.0, 147.5, 145.8, and 145.5 (all s, C$_{q-IPr}$), 136.9 and 136.7 (both s, C$_q$N), 129-122 (CH$_{Ph-IPr}$), 128.7 and 126.8 (both s, HC=CH$_{pht}$), 124.4 and 124.1 (both s, =CHN), 60.1 and 59.2 (d, J_{C-Rh} = 15.7, =CH$_{coe}$), 41.5 and 40.7 (both s, CH$_{pht}$), 31.3 and 26.6 (both s, CH$_{2-pht}$), 29.7, 29.6, 28.0, 27.9, 26.6, and 23.7 (all s, CH$_{2-coe}$), 28.7, 28.6, 28.5 and 28.5 (all s, CHMe$_{IPr}$), 26.7, 26.6, 26.3, 26.2, 22.9, 22.5, 22.4, and 21.7 (all s, Me$_{IPr}$).

Preparation of Rh{κ^2*N,O*-(C$_5$H$_8$NO)}(η^2-coe)(IPr) (13). This complex was prepared as described for **3** starting from 2-piperidone (32 mg, 0.32 mmol), KO^{t}Bu (35 mg, 0.31 mmol) and **1** (200 mg, 0.16 mmol). Yield: 154 mg (65%), yellow solid. Anal. calcd for C$_{40}$H$_{58}$N$_3$ORh: C, 68.65; H, 8.35; N, 6.00. Found: C, 68.41; H, 8.35; N, 5.90. IR (cm^{-1}, ATR): 1566 ν(OCN$_{sym}$), 1462 ν(OCN$_{asym}$). ^{1}H NMR (300.1 MHz, C$_6$D$_6$, 298 K): δ 7.28 (m, 6H, H$_{Ph-IPr}$), 6.52 (s, 2H, =CHN), 3.21 (sept, J_{H-H} = 6.8, 4H, CHMe$_{IPr}$), 2.75 (t, J_{H-H} = 5.7, 2H, CH$_{2-pip-6}$), 2.64 (m, 2H, =CH$_{coe}$), 1.93 (t, J_{H-H} = 6.5, 2H, CH$_{2-pip-3}$), 1.9-1.0 (m, 12H, CH$_{2-coe}$), 1.59 and 1.09 (both d, J_{H-H} = 6.8, 24H, Me$_{IPr}$), 1.29 (m, 2H, CH$_{2-pip-4}$), 1.11 (m, 2H, CH$_{2-pip-5}$). ^{13}C{^{1}H}-APT NMR (100.5 MHz, C$_6$D$_6$, 298 K): δ 187.8 (d, J_{C-Rh} = 58.8, Rh-C$_{IPr}$), 181.6 (d, J_{C-Rh} = 3.1, C$_{2-pip}$), 147.1 (s, C$_{q-IPr}$), 137.7 (s, C$_q$N), 129.7 (s, CH$_{p-Ph-IPr}$), 124.2 (s, =CHN), 123.9 (s, CH$_{m-Ph-IPr}$), 55.6 (d, J_{C-Rh} = 16.8, =CH$_{coe}$), 44.9 (s, C$_{6-pip}$), 30.6 (s, C$_{3-pip}$), 30.5, 30.4, and 27.2 (all s, CH$_{2-coe}$), 29.0 (s, CHMe$_{IPr}$), 26.5 and 23.2 (both s, Me$_{IPr}$), 23.8 (s, C$_{5-pip}$), 21.5 (s, C$_{4-pip}$). ^{15}N HMQC (long range) NMR (40.5 MHz, C$_6$D$_6$, 298 K): δ 191.1 (N$_{IPr}$), 143.4 (N$_{pip}$).

In situ formation of Rh{κ^2*N,O*-(6-Me-Opy)}{η^2-(3-hexyne)}(IPr) (14a). This complex was prepared from **5** (20 mg, 0.03 mmol) in C$_6$D$_6$ at 298 K (0.5 mL, NMR tube) and 3-hexyne (4 μL, 0.03 mmol). HRMS (ESI+): m/z Calcd for C$_{39}$H$_{52}$N$_3$ORh: [M-H+O]$^+$: 696.3030. Exp: 696.3048. ^{1}H NMR (400 MHz, C$_6$D$_6$, 298 K): δ 7.3-7.2 (6H, H$_{Ph-IPr}$), 6.84 (dd, J_{H-H} = 8.4, 7.2, 1H, H$_{4-Opy}$), 6.42 (s, 2H, =CHN), 5.82 (d, J_{H-H} = 8.4, 1H, H$_{3-Opy}$), 5.66 (d, J_{H-H} = 7.2, 1H, H$_{5-Opy}$), 3.26 (sept, J_{H-H} = 6.9, 4H, CHMe$_{IPr}$), 2.19 and 1.72 (both m, 4H, CH$_{2-hexyne}$), 1.68 (s, 3H, Me$_{Opy}$), 1.62 and 1.10 (both d, J_{H-H} = 6.8, 24H, Me$_{IPr}$), 1.12 (t, J_{H-H} = 7.2, 6H, CH$_{3-hexyne}$). ^{13}C{^{1}H}-APT NMR (100.5 MHz, C$_6$D$_6$, 298 K): δ 184.8 (d, J_{C-Rh} = 61.0, Rh-C$_{IPr}$), 181.0 (d, J_{C-Rh} = 2.9, C$_{2-Opy}$), 154.8 (s, C$_{6-Opy}$), 147.2 (s, C$_{q-IPr}$), 138.4 (s, C$_{4-Opy}$), 137.8 (s, C$_q$N), 129.4 and 124.0 (both s, CH$_{Ph-IPr}$), 124.3 (s, =CHN), 108.4 (s, C$_{5-Opy}$), 106.8 (s, C$_{3-Opy}$), 73.2 (d, J_{C-Rh} = 16.9, Rh-C≡C), 29.2 (s, CHMe$_{IPr}$), 26.0 and 23.7 (both s, Me$_{IPr}$), 20.6 (s, Me$_{Opy}$), 18.9 (s, CH$_{2-hexyne}$), 14.6 (s, CH$_{3-hexyne}$). ^{1}H-^{15}N HMQC (long range) NMR (40.5 MHz, C$_6$D$_6$, 298 K): δ 208.6 (N$_{Opy}$), 189.1 (N$_{IPr}$).

Standard Conditions for the Catalytic Alkyne Dimerization. To a C$_6$D$_6$ solution (0.5 mL) in a NMR tube under argon atmosphere, 0.01 mmol of catalyst and 0.17 mmol of mesitylene as internal standard were added. The solution was frozen by means of a dewar flask containing isopropanol at 195 K. Then, 0.50 mmol of alkyne were added and the NMR tube was sealed under argon. The tube was allowed to warm up to room temperature just before the first NMR spectrum was recorded. The reaction course was monitored by ^{1}H NMR spectroscopy and the conversion was determined by integration of the corresponding resonances of the internal standard and the products. For 0.1 or 0.05 mol% catalyst loading experiments, a 20 mM solution of catalyst in C$_6$D$_6$ was prepared and then, the corresponding amount of this solution was added to the reaction mixture and it was proceeded as described above.

Crystal Structure Determination. Single crystals of **5**, **7**, **10**, **11**, and **13** were obtained by slow diffusion of hexane into C$_6$D$_6$ (**5**, **7**, and **10**) or toluene solutions (**11** and **13**). X-ray diffraction data were collected at 100(2) K on a SMART APEX (**13**) or D8 VENTURE (**5**, **7**, **10**, and **11**) Bruker diffractometers with graphite-monochromated Mo−Kα radiation (λ = 0.71073 Å) using ω-scans (and φ-scans for **5**, **7**, **10**, and **11**). Intensities were integrated and corrected for absorption effects with SAINT–PLUS[27] and SADABS[28] programs, both included in APEX4 package. The structures were solved by the Patterson method with SHELXS-97[29] and refined by full matrix least-squares on F2 with SHELXL-2014[30] under WinGX.[31]

Crystal data and structure refinement for 5. C$_{41}$H$_{56}$N$_3$ORh, 709.79 g·mol^{-1}, monoclinic, $P2_1/c$, a = 11.2776(3) Å, b = 11.0342(3) Å, c = 29.2518(9) Å, β = 91.8430(10)°, V = 3638.19(18) Å^3, Z = 4, D_{calc} = 1.296 g·cm^{-3}, μ = 0.504 mm^{-1}, F(000) = 1504, orange prism, 0.220 x 0.120 x 0.050 mm^3, $\theta_{min}/\theta_{max}$ 2.246/28.706°, index ranges –14≤h≤15, –14≤k≤14, –39≤l≤39, reflections collected/independent 86793/9410 [R(int) = 0.0437], T_{max}/T_{min} 0.7458/0.7077, data/restraints/parameters 9410/0/424, GooF(F^2) = 1.101, R_1 = 0.0394 wR_2 = 0.0911 (all data), largest diff. peak/hole 1.546/–0.864 e·Å^{-3}. CCDC deposit number 2364401.

Crystal data and structure refinement for 7. C$_{41}$H$_{55}$BrCl$_2$N$_3$ORh, 859.60 g·mol^{-1}, monoclinic, a = 18.8489(9) Å, b = 10.6452(5) Å, c = 20.9338(10) Å, β = 107.430(2)°, V = 4007.5(3) Å^3, Z = 4, D_{calc} = 1.425 g·cm^3, μ = 1.591 mm^{-1}, F(000) = 1776, orange prism, 0.190 x 0.180 x 0.120 mm^3, $\theta_{min}/\theta_{max}$ 2.014/28.722°, index ranges –25≤h≤25, –14≤k≤14, –28≤l≤28, reflections collected/independent 176700/10376 [R(int) = 0.0461], T_{max}/T_{min} 0.7458/0.6850, data/restraints/parameters 10376/0/424, GooF(F^2) = 1.043, R_1 = 0.0276 [I>2σ(I)], wR_2 = 0.0714 (all data), largest diff. peak/hole 0.961/–0.313 e·Å^{-3}. CCDC deposit number 2364402.

Crystal data and structure refinement for 10. C$_{39}$H$_{53}$N$_4$ORh, 696.76 g·mol^{-1}, monoclinic, $P2_1/c$, a = 11.0993(6) Å, b = 10.5668(6) Å, c = 30.1434(16) Å, β = 90.330(2)°, V = 3535.3(3) Å^3, Z = 4, D_{calc} = 1.309 g·cm^3, μ = 0.518 mm^{-1}, F(000) = 1472, orange prism, 0.200 x 0.175 x 0.120 mm^3, $\theta_{min}/\theta_{max}$ 2.042/28.731°, index ranges –14≤h≤15, –13≤k≤14, –40≤l≤40, reflections collected/independent 98444/9151 [R(int) = 0.0391], T_{max}/T_{min} 0.7457/0.6853, data/restraints/parameters 9151/40/457, Goof(F^2) = 1.273, R_1 = 0.0540 [I>2σ(I)], wR_2 = 0.1149 (all data), largest diff. peak/hole 1.013/–1.369 e·Å^{-3}. CCDC deposit number 2364400.

Crystal data and structure refinement for 11. C$_{51}$H$_{66}$N$_3$O$_2$Rh, 855.97 g·mol^{-1}, monoclinic, $C2/c$, a = 46.591(2) Å, b = 10.9772(5) Å, c = 18.6924(8) Å, β = 110.104(3)°, V = 8977.4(7) Å^3, Z = 8, D_{calc} = 1.267 g·cm^3, μ = 0.422 mm^{-1}, F(000) = 3632, orange prism, 0.180 x 0.120 x 0.080 mm^3, $\theta_{min}/\theta_{max}$ 2.153/28.732°, index ranges –62≤h≤62, –14≤k≤14, –25≤l≤25, reflections collected/independent 306549/11639 [R(int) = 0.0373], T_{max}/T_{min} 0.7458/0.7012, data/restraints/parameters 11639/13/559, GooF(F^2) = 1.054, R_1 = 0.0236 [I>2σ(I)], wR2 = 0.0591 (all data), largest diff. peak/hole 0.417/–0.319 e·Å^{-3}. CCDC deposit number 2364403.

Crystal data and structure refinement for 13. C$_{40}$H$_{58}$N$_3$ORh, 699.80 g·mol^{-1}, monoclinic, $P2_1/n$, a = 10.1740(9) Å, b = 31.683(3) Å, c = 11.4151(10) Å, β = 91.7630(10)°, V = 3677.9(6) Å^3, Z = 4, D_{calc} = 1.264 g·cm^3, μ = 0.498 mm^{-1}, F(000) = 1488, orange prism, 0.350 x 0.240 x 0.090 mm^3, $\theta_{min}/\theta_{max}$ 2.103/28.419°, index ranges –13≤h≤13, –41≤k≤42, –15≤l≤15, reflections collected/independent 44100/9068 [R(int) = 0.0580], T_{max}/T_{min} 0.9020/0.8245, data/restraints/parameters 9068/27/433, GooF(F^2) = 1.041, R_1 = 0.0399 [I>2σ(I)], wR_2 = 0.0765 (all data), largest diff. peak/hole 0.616/–0.760 e·Å^{-3}. CCDC deposit number 2364399.

Computational details. All DFT theoretical calculations were carried out using the Gaussian program package.[32] Energies, gradients and frequency analysis was performed using the B97D3 functional[33] in combination to the def2-SVP basis set[34] which include effective core potentials for Rh. Energies were refined by M06L/def2-TZVP single point calculations[35] using the SMD approach[36] for benzene as implemented in G09. The "ultrafine" grid was employed in all calculations. All reported energies are Gibbs free energies referred to a 1 M standard state using the correction proposed by Goddard III et al.[37] at 25 ºC including basis set and solvent corrections. The nature of the stationary points was confirmed by analytical frequency analysis, and transition states were characterized by a single imaginary frequency corresponding to the expected motion of the atoms.

ASSOCIATED CONTENT

Supporting Information

The Supporting Information is available free of charge on the ACS Publications website

Miscellaneous information including NMR data of complexes and organic products, and DFT calculation data (PDF)

Optimized coordinates for the computed compounds (XYZ)

AUTHOR INFORMATION

Corresponding Author

Dr. Ricardo Castarlenas – *Departamento de Química Inorgánica – Instituto de Síntesis Química y Catálisis Homogénea (ISQCH), Universidad de Zaragoza – CSIC, C/ Pedro Cerbuna 12, 50009 Zaragoza, Spain*; Orcid.org/0000-0003-4460-8678. Email: rcastar@unizar.es

Authors

Belinda Español-Sánchez – *Departamento de Química Inorgánica – Instituto de Síntesis Química y Catálisis Homogénea (ISQCH), Universidad de Zaragoza – CSIC, C/ Pedro Cerbuna 12, 50009 Zaragoza, Spain;* Orcid.org/0000-0001-6461-3592.

Dr. María Galiana-Cameo – *Departamento de Química Inorgánica – Instituto de Síntesis Química y Catálisis Homogénea (ISQCH), Universidad de Zaragoza – CSIC, C/ Pedro Cerbuna 12, 50009 Zaragoza, Spain;* Orcid.org/0000-0002-2043-4864.

Dr. Asier Urriolabeitia – *Departamento de Química Física, Universidad de Zaragoza, C/Pedro Cerbuna 12, 50009 Zaragoza, Spain;* Orcid.org/0000-0001-9352-6922.

Prof. Víctor Polo – *Departamento de Química Física, Universidad de Zaragoza, C/Pedro Cerbuna 12, 50009 Zaragoza, Spain*, Orcid.org/0000-0001-5823-7965.

Dr. Vincenzo Passarelli – *Departamento de Química Inorgánica – Instituto de Síntesis Química y Catálisis Homogénea (ISQCH), Universidad de Zaragoza – CSIC, C/ Pedro Cerbuna 12, 50009 Zaragoza, Spain*; Orcid.org/0000-0002-1735-6439.

Prof. Jesús J. Pérez Torrente – *Departamento de Química Inorgánica – Instituto de Síntesis Química y Catálisis Homogénea (ISQCH), Universidad de Zaragoza – CSIC, C/ Pedro Cerbuna 12, 50009 Zaragoza, Spain*; Orcid.org/0000-0002-3327-0918.

Notes

The authors declare no competing financial interest

ACKNOWLEDGMENT

Financial support from the Spanish Ministry of Science and Innovation MCIN/AEI/10.13039/501100011033, under the Projects PID2019-103965GB-I00 and PID2022-137208NB-I00, and the Departamento de Educación, Ciencia y Universidades del Gobierno de Aragón (group E42_23R) is gratefully acknowledged. A.U. thankfully acknowledges the Spanish MECD for a FPU fellowship (FPU 2017/05417). Authors would like to acknowledge the use of Servicio General de Apoyo a la Investigación-SAI, Universidad de Zaragoza and the computational resources provided by the Institute for Biocomputation and the Physics of Complex Systems (BIFI) – Universidad de Zaragoza.

REFERENCES

(1) Grover, J.; Prakash, G.; Goswamil, N.; Maiti, D. Traditional and Sustainable Approaches for the Construction of C–C Bonds by Harnessing C–H Arylation. *Nat. Commun.* **2022**, *13*, 1085-1102.

(2) Altus, K. M.; Love, J. A. The Continuum of Carbon–Hydrogen (C–H) Activation Mechanisms and Terminology. *Commun. Chem.* **2021**, *4*, 173.

(3) (a) Gorelsky, S. I.; Lapointe, D.; Fagnou, K. Analysis of the Concerted Metalation-Deprotonation Mechanism in Palladium-Catalyzed Direct Arylation Across a Broad Range of Aromatic Substrates. *J. Am. Chem. Soc.* **2008**, *130*, 10848-10849. (b) Davies, D. L.; Macgregor, S. A.; McMullin, C. L. Computational Studies of Carboxylate-Assisted C−H Activation and Functionalization at Group 8−10 Transition Metal Centers. *Chem. Rev.* **2017**, *117*, 8649-8709.

(4) Perutz, R. N.; Sabo-Etienne, S.; Weller A. S. Metathesis by Partner Interchange in s-Bond Ligands: Expanding Applications of the s-CAM Mechanismσ. *Angew. Chem. Int. Ed.* **2022**, *61*, e202111462.

(5) Guihaumé, J.; Halbert, S.; Eisenstein, O.; Perutz R. N. Hydrofluoroarylation of Alkynes with Ni Catalysts. C−H Activation via Ligand-to-Ligand Hydrogen Transfer, an Alternative to Oxidative Addition. *Organometallics* **2012**, *31*, 1300-1314.

(6) Yi, H.; Zhang, G.; Wang, H.; Huang, Z.; Wang, J.; Singh, A. K.; Lei, A. Recent Advances in Radical C−H Activation/Radical Cross-Coupling. *Chem. Rev.* **2017**, *117*, 9016-9085.

(7) Singh, S.; Hazra, C. K. Outer-Sphere C-H Bond Activation. In Handbook of C-H Functionalization. Maiti, D. Ed. Wiley, New York **2022**.

(8) Higashi, T.; Kusumoto, S.; Nozaki, K. Cleavage of Si-H, B-H, and C-H bonds by Metal-Ligand Cooperation. *Chem. Rev.* **2019**, *119*, 10393-10402.

(9) Yue, H.; Zhu, C.; Kancherla, R.; Liu, F.; Rueping, M. Regioselective Hydroalkylation and Arylalkylation of Alkynes by Photoredox/Nickel Dual Catalysis: Application and Mechanism. *Angew. Chem. Int. Ed.* **2020**, *59*, 5738-5746.

(10) Johnson, D. G.; Lynam, J. M.; Slattery, J. M.; Welby, C. E. Insights into the Intramolecular Acetate-Mediated Formation of Ruthenium Vinylidene Complexes: a Ligand-Assisted Proton Shuttle (LAPS) Mechanism. *Dalton Trans.* **2010**, *39*, 10432-10441.

(11) (a) Jiménez-Tenorio, M.; Puerta, M. C.; Valerga, P.; Ortuño, M. A.; Ujaque, G.; Lledós, A. Counteranion and Solvent Assistance in Ruthenium-Mediated Alkyne to Vinylidene Isomerizations. *Inorg. Chem.* **2013**, *52*, 8919-8932. (b) Breit, B.; Gellrich, U.; Li, T.; Lynam, J. M.; Milner, L. M.; Pridmore, N. E.; Slattery, J. M.; Whitwood, A. C. Mechanistic Insight into the Ruthenium-Catalysed anti-Markovnikov Hydration of Alkynes Using a Self-Assembled Complex: a Crucial Role for Ligand-Assisted Proton Shuttle Processes. *Dalton Trans.* **2014**, *43*, 11277-11285. (c) Leeb, N. M.; Drover, M. W.; Love, J. A.; Schafer, L. L.; Slattery, J. M. Phosphoramidate-Assisted Alkyne Activation: Probing the Mechanism of Proton Shuttling in a N,O-Chelated Cp*Ir(III) Complex. *Organometallics* **2018**, *37*, 4630-4638.

(12) See for example: (a) Scrivanti, A.; Beghetto, V.; Campagna, E.; Zanato, M.; Matteoli, U. Mechanism of the Alkoxycarbonylation of Alkynes in the Presence of the $Pd(OAc)_2/PPh_2Py/CH_3SO_3H$ Catalytic System. *Organometallics* **1998**, *17*, 630-635. (b) Jeanne-Julien L.; Masson, G.; Kouoi, R.; Regazzetti, A.; Genta-Jouve, G.; Gandon, V.; Roulland, E. Stereoselective Access to (E)-1,3-Enynes through Pd/Cu-Catalyzed Alkyne Hydrocarbation of Allenes. *Org. Lett.* **2019**, *21*, 3136-3141. (c) Virant M.; Mihelač, M.; Gazvoda, M.; Cotman, A. E.; Frantar, A.; Pinter, B.; Košmrlj. Pyridine Wingtip in $[Pd(PytzNHC)_2]_2^+$ Complex Is a Proton Shuttle in the Catalytic Hydroamination of Alkynes. *Org. Lett.* **2020**, *22*, 2157-2161. (d) Corpas, J.; Arpa, E. M.; Lapierre, R.; Corral, I.; Mauleon, P.; Gómez-Arrayas, R.; Carretero, J. C. Interplay between the Directing Group and Multifunctional Acetate Ligand in Pd-Catalyzed anti-Acetoxylation of Unsymmetrical Dialkyl-Substituted Alkynes. *ACS Catal.* **2022**, *12*, 6596-6605. (e) Andrés, J. L.; Suarez, E.; Martin, M.; Sola, E. Mechanistic Versatility at Ir(PSiP) Pincer Catalysts: Triflate Proton Shuttling from 2-Butyne to Diene and [3]Dendralene Motifs. *Organometallics* **2022**, *41*, 2622-2630. (f) Jannsen, N.; Reiß, F.; Drexler, H.-J.; Konieczny, K.; Beweries, T.; Heller, D. The Mechanism of Rh(I)-Catalyzed Coupling of Benzotriazoles and Allenes Revisited: Substrate Inhibition, Proton Shuttling, and the Role of Cationic vs Neutral Species. *J. Am. Chem. Soc.* **2024**, *146*, 12185-12196

(13) (a) Galiana-Cameo, M.; Borraz, M.; Zelenkova, Y.; Passarelli, V.; Lahoz, F. J.; Pérez-Torrente, J. J.; Oro, L. A.; Di Giuseppe, A.;

Castarlenas, R. Rhodium(I)-NHC Complexes Bearing Bidentate Bis-Heteroatomic Acidato Ligands as *gem*-Selective Catalysts for Alkyne Dimerization. *Chem. Eur. J.* **2020**, *26*, 9598-9608. (b) Galiana-Cameo, M.; Urriolabeitia, A.; Barrenas, E.; Passarelli, V.; Pérez-Torrente, J. J.; Di Giuseppe, A.; Polo, V.; Castarlenas, R. Metal−Ligand Cooperative Proton Transfer as an Efficient Trigger for Rhodium-NHC-Pyridonato Catalyzed *gem*-Specific Alkyne Dimerization. *ACS Catal.* **2021**, *11*, 7553-7567.

(14) (a) Trost, B. M.; Masters, J. T. Transition Metal-Catalyzed Couplings of Alkynes to 1,3-Enynes: Modern Methods and Synthetic Applications. *Chem. Soc. Rev.* **2016**, *45*, 2212-2238. (b) Liang, Q.; Hayashi, K.; Song, D. Catalytic Alkyne Dimerization without Noble Metals. *ACS Catal.* **2020**, *10*, 4895-4905. (c) Weber, S. M.; Hilt, G. Late 3d Metal-Catalyzed (Cross-) Dimerization of Terminal and Internal Alkynes. *Front. Chem.* **2021**, *9*, 635826.

(15) Rubio-Pérez, L.; Azpíroz, R.; Di Giuseppe, A.; Polo, V.; Castarlenas, R.; Pérez-Torrente, J. J.; Oro, L. A. Pyridine-Enhanced Head-to-Tail Dimerization of Terminal Alkynes by a Rhodium–N-Heterocyclic-Carbene Catalyst. *Chem. Eur. J.* **2013**, *19*, 15304-15314.

(16) See for example: (a) Haskel, A.; Straub, T.; Dash, A. K.; Eisen, M. S. Oligomerization and Cross-Oligomerization of Terminal Alkynes Catalyzed by Organoactinide Complexes. *J. Am. Chem. Soc.* **1999**, *121*, 3014-3024. (b) Platel, R. H.; Schafer, L. L. Zirconium Catalyzed Alkyne Dimerization for Selective Z-Enyne Synthesis. *Chem. Commun.* **2012**, *48*, 10609-10611. (c) Chen, T.; Guo, C.; Goto, M.; Han, L.-B. A Brønsted Acid-Catalyzed Generation of Palladium Complexes: Efficient Head-to-Tail Dimerization of Alkynes. *Chem. Commun.* **2013**, *49*, 7498-7500. (d) Zatolochnaya, O. V.; Gordeev, E. G.; Jahier, C.; Ananikov, V. P.; Gevorgyan, V. Carboxylate Switch between Hydro- and Carbopalladation Pathways in Regiodivergent Dimerization of Alkynes. *Chem. Eur. J.* **2014**, *20*, 9578-9588. (e) Salvio, R.; Juliá-Hernández, F.; Pisciottani, L.; Mendoza-Meroño, R.; García-Granda, S.; Bassetti, M. Kinetics and Mechanistic Insights into the Acetate-Assisted Dimerization of Terminal Alkynes under Ruthenium- and Acid-Promoted (RAP) Catalysis. *Organometallics* **2017**, *36*, 3830-3840. (f) Żak, P.; Bołt, M.; Lorkowski, J.; Kubicki, M.; Pietraszuk, C. Platinum Complexes Bearing Bulky N-Heterocyclic Carbene Ligands as Efficient Catalysts for the Fully Selective Dimerization of Terminal Alkynes. *ChemCatChem* **2017**, *9*, 3627-3631. (g) Storey, C. M.; Gyton, M. R.; Andrew, R. E.; Chaplin, A. B. Terminal Alkyne Coupling Reactions through a Ring: Mechanistic Insights and Regiochemical Switching. *Angew. Chem. Int. Ed.* **2018**, *57*, 12003-12006. (h) Liang, Q.; Sheng, K.; Salmon, A.; Zhou, V. Y.; Song, D. Active Iron(II) Catalysts toward gem-Specific Dimerization of Terminal Alkynes. *ACS Catal.* **2019**, *9*, 810-818. (i) Zhuang, X.; Chen, J.-Y.; Z. Yang, Z.; Jia, M.; Wu, C.; Liao, R.-Z.; Tung, C.-H.; Wang, W. Sequential Transformation of Terminal Alkynes to 1,3-Dienes by a Cooperative Cobalt Pyridonate Catalyst. *Organometallics* **2019**, *38*, 3752-3759. (j) Hasenbeck, M.; Müller, T.; Gellrich, U. Metal-free gem Selective Dimerization of Terminal Alkynes Catalyzed by a Pyridonate Borane Complex. *Catal. Sci. Tech.* **2019**, *9*, 2438-2444. (k) Ueda, Y.; Tsurugi, H.; Mashima, K. Cobalt-Catalyzed E-Selective Cross-Dimerization of Terminal Alkynes: A Mechanism Involving Cobalt(0/II) Redox Cycles. *Angew. Chem. Int. Ed.* **2020**, *59*, 1552-1556. (l) Chen, J.-F.; Li, C. Cobalt-Catalyzed gem-Cross-Dimerization of Terminal Alkynes. *ACS Catal.* **2020**, *10*, 3881-3889. (m) Pfeffer, C.; Wannenmacher, N.; Frey, W. Peters, R. Stereo- and Regioselective Dimerization of Alkynes to Enynes by Bimetallic Syn-Carbopalladation. *ACS Catal.* **2021**, *11*, 5496-5505. (n) Weber, S.; Veiros, L. F.; Kirchner, K. Selective Manganese-Catalyzed Dimerization and Cross-Coupling of Terminal Alkynes. *ACS Catal.* **2021**, *11*, 6474-6483. (o) Sun, Y.; Zhang, J.; Zeng, Y.; Meng L.; Li, X. Mechanism and Stereoselectivity Control of Terminal Alkyne Dimerization Activated by a Zr/Co Heterobimetallic Complex: A DFT Study. *J. Org. Chem.* **2024**, *89*, 605-616. (p) de las Heras, L. A.; Esteruelas, M. A.; Oliván, M.; Oñate, E. Homo- and Cross-Coupling of Phenylacetylenes and α-Hydroxyacetylenes Catalyzed by a Square-Planar Rhodium Monohydride. *ACS Catal.* **2024**, *14*, 8389-8404. (q) Stevens, J. E.; Miller, J. D.; Fitzsimmons, M. C.; Moore, C. E.; Thomas, C. M. Z-selective dimerization of terminal alkynes by a (PNNP)Fe^{II} complex. *Chem. Commun.* **2024**, *60*, 5169-5172.

(17) Chen, J.; Wei, W.-T.; Li, Z.; Lu, Z. Metal-Catalyzed Markovnikov-Type Selective Hydrofunctionalization of Terminal Alkynes. *Chem. Soc. Rev.* **2024**, *53*, 7566-7589.

(18) (a) Gellrich, U.; Meiβner, A.; Steffani, A.; Kähny, M.; Drexler, H.-J.; Heller, D.; Plattner, D. A.; Breit, B. Mechanistic Investigations of the Rhodium Catalyzed Propargylic CH Activation. *J. Am. Chem. Soc.* **2014**, *136*, 1097-1104. (b) Ahmad, S.; Lockett, A.; Shuttlewoth, T. A.; Miles-Hobbs, A. M.; Pringle, P. G.; Bühl, M. Palladium-Catalysed Alkyne Alkoxycarbonylation with P,N-Chelating Ligands Revisited: a Density Functional Theory Study. *Phys. Chem. Chem. Phys.* **2019**, *21*, 8543–8552. (c) Galiana-Cameo, M.; Romeo, R.; Urriolabeitia, A.; Passarelli, V.; Pérez-Torrente, J. J.; Polo, V.; Castarlenas, R. Rhodium-NHC-Catalyzed *gem*-Specific *O*-Selective Hydropyridonation of Terminal Alkynes. *Angew. Chem. Int. Ed.* **2022**, *61*, e202117006.

(19) (a) Rawson, J. M.; Winpenny, R. E. P. The Coordination Chemistry of 2-pyridone and its Derivatives. *Coord. Chem. Rev.* **1995**, *139*, 313-374. (b) Dorver, M. W.; Love, J. A.; Schafer, L. L. 1,3-N,O-Complexes of Late Transition Metals. Ligands with Flexible Bonding Modes and Reaction Profiles. *Chem. Soc. Rev.* **2017**, *49*, 2913–2940. (c) Fedulin A.; von Wangelin, A. J. 2-Pyridonates: a Versatile Ligand Platform in 3d Transition Metal Coordination Chemistry and Catalysis. *Catal. Sci. Technol.* **2024**, *14*, 26–42.

(20) (a) Di Giuseppe, A.; Castarlenas, R.; Pérez-Torrente, J. J.; Crucianelli, M.; Polo, V.; Sancho, R.; Lahoz, F. J.; Oro, L. A. Ligand-Controlled Regioselectivity in the Hydrothiolation of Alkynes by Rhodium N-Heterocyclic Carbene Catalysts. *J. Am. Chem. Soc.* **2012**, *134*, 8171. (b) Palacios, L.; Artigas, M. J.; Polo, V.; Lahoz, F. J.; Castarlenas, R.; Pérez-Torrente, J. J.; Oro, L. A. Hydroxo−Rhodium−N-Heterocyclic Carbene Complexes as Efficient Catalyst Precursors for Alkyne Hydrothiolation. *ACS Catal.* **2013**, *3*, 2910-2919. (c) Palacios, L.; Di Giuseppe, A.; Artigas, M. J.; Polo, V.; Lahoz, F. J.; Castarlenas, R.; Pérez-Torrente, J. J.; Oro, L. A. Mechanistic Insight into the Pyridine Enhanced α-Selectivity in Alkyne Hydrothiolation Catalysed by Quinolinolate–Rhodium(I)–N-heterocyclic Carbene Complexes. *Catal. Sci. Technol.* **2016**, *6*, 8548-8561. (d) Palacios, L.; Meheut, Y.; Galiana-Cameo, M.; Artigas, M. J.; Di Giuseppe, A.; Lahoz, F. J.; Polo, V.; Castarlenas, R.; Pérez-Torrente, J. J.; Oro, L. A. Design of Highly Selective Alkyne Hydrothiolation Rh^{I}-NHC Catalysts: Carbonyl-Triggered Nonoxidative Mechanism. *Organometallics* **2017**, *36*, 2198-2207. (e) Hermosilla, P.; Funes-Hernando, D.; Castarlenas, R.; Di Giuseppe, A.; Azpíroz, R.; Vispe, E.; Pérez-Torrente, J. J. Tailor-Made Poly(Vinylidene Sulfide)s by Rh(I)–NHC Catalyzed Regioselective Thiol-yne Click Polymerization. *Eur. Polym. J.* **2023**, *194*, 112117.

(21) (a) Azpíroz, R.; Rubio-Pérez, L.; Castarlenas, R.; Pérez-Torrente, J. J.; Oro, L. A. gem-Selective Cross-Dimerization and Cross-Trimerization of Alkynes with Silylacetylenes Promoted by a Rhodium–Pyridine–N-Heterocyclic Carbene Catalyst. *ChemCatChem* **2014**, *6*, 2587-2592. (b) Kleinhans, G.; Guisado-Barrios, G.; Liles, D. C.; Bertrand, G. Bezuidenhout, D. I. A Rhodium(I)–Oxygen Adduct as a Selective Catalyst for One-Pot Sequential Alkyne Dimerization-Hydrothiolation Tandem Reactions. *Chem. Commun.* **2016**, *52*, 3504-3507. (c) Storey, C. M.; Gytin, M. R.; Andrew, R. E.; Chaplin, A. B. Terminal Alkyne Coupling Reactions Through a Ring: Effect of Ring Size on Rate and Regioselectivity. *Chem. Eur. J.* **2020**, *26*, 14715-14723.

(22) Yu, X.-Y.; Patrick, B. O.; James, B. R. Rhodium(III) Peroxo Complexes Containing Carbene and Phosphine Ligands. *Organometallics* **2006**, *25*, 4870-4877.

(23) (a) Palacios, L.; Di Giuseppe, A.; Castarlenas, R.; Lahoz, F. J.; Pérez-Torrente, J. J.; Oro, L. A. Pyridine versus Acetonitrile Coordination in Rhodium–N-Heterocyclic Carbene Square-Planar Complexes. *Dalton Trans.* **2015**, *44*, 5777-5789. (b) Fuertes, S.; Chueca, A.; Sicilia, V. Exploring the Transphobia Effect on Heteroleptic NHC Cycloplatinated Complexes. *Inorg. Chem.* **2015**, *54*, 9885-9895.

(24) Zenkina, O. V.; Keske, E. C.; Kochhar, G. S.; Wang, R.; Crudden, C. M. Heteroleptic Rhodium NHC Complexes with Pyridine Derived Ligands: Synthetic Accessibility and Reactivity Towards Oxygen. *Dalton Trans.* **2013**, *42*, 2282-22293.

(25) (a) Masciocchi, N.; Ardizzoia, G. A.; LaMonica, G.; Maspero, A.; Sironi, A. Thermally Robust Metal Coordination Polymers: The

Cobalt, Nickel, and Zinc Pyrimidin-2-olate Derivatives. *Eur. J. Inorg. Chem.* **2000**, 2507-2505. (b) Kurishima, S.; Matsuda, N.; Tamura, N.; Ito, T. Bidentate Cyclic Imido Complexes of Molybdenum(II). Preparation, Solution Behaviour and X-Ray Crystal Structure. *Dalton Trans.* **1991**, 1135-1141. (c) Zhong, H.; Egger, D. T.; Gasser, V. C. M.; Finkelstein; P.; Keim, L.; Seidel, M. Z.; Trapp, N.; Morandi, B. Skeletal Metalation of Lactams through a Carbonyl-to-Nickel-Exchange Logic. *Nat. Commun.* **2023**, *14*, 5273.

(26) Kozuch, S.; Shaik, S. How to Conceptualize Catalytic Cycles? The Energetic Span Model. *Acc. Chem. Res.* **2011**, *44*, 101-110.

(27) *SAINT+: Area-Detector Integration Software*, version 6.01; Bruker AXS: Madison, WI, 2001.

(28) Sheldrick, G. M. SADABS *program*; University of Göttingen: Göttingen, Germany, 1999.

(29) Sheldrick, G. M. *SHELXS 97, Program for the Solution of Crystal Structure*; University of Göttingen: Göttingen, Germany, 1997.

(30) Sheldrick, G. M. Crystal structure refinement with SHELXL. *Acta Cryst., Sect. C: Struct. Chem.* **2015**, *71*, 3−8.

(31) Farrugia, L. J. WinGX and ORTEP for Windows: An Update. *J. Appl. Cryst.* **2012**, ***45***, 849−854.

(32) Schlegel, H. B.; Scuseria, G. E.; Robb, M. A.; Cheeseman, J. R.; Scalmani, G.; Barone, V.; Petersson, G. A.; Nakatsuji, H.; Li, X.; Caricato, M.; Marenich, A. V.; Bloino, J.; Janesko, B. G.; Gomperts, R.; Mennucci, B.; Hratchian, H. P.; Ortiz, J. V.; Izmaylov, A. F.; Sonnenberg, J. L.; Williams-Young, D.; Ding, F.; Lipparini, F.; Egidi, F.; Goings, J.; Peng, B.; Petrone, A.; Henderson, T.; Ranasinghe, D.; Zakrzewski, V. G.; Gao, J.; Rega, N.; Zheng, G.; Liang, W.; Hada, M.; Ehara, M.; Toyota, K.; Fukuda, R.; Hasegawa, J.; Ishida, M.; Nakajima, T.; Honda, Y.; Kitao, O.; Nakai, H.; Vreven, T.; Throssell, K.; Montgomery, J. A., Jr.; Peralta, J. E.; Ogliaro, F.; Bearpark, M. J.; Heyd, J. J.; Brothers, E. N.; Kudin, K. N.; Staroverov, V. N.; Keith, T. A.; Kobayashi, R.; Normand, J.; Raghavachari, K.; Rendell, A. P.; Burant, J. C.; Iyengar, S. S.; Tomasi, J.; Cossi, M.; Millam, J. M.; Klene, M.; Adamo, C.; Cammi, R.; Ochterski, J. W.; Martin, R. L.; Morokuma, K.; Farkas, O.; Foresman, J. B.; Fox, D. J. Gaussian, Inc., Wallingford CT, 2016.

(33) (a) Becke, A. D. Density-Functional Thermochemistry. V. Systematic Optimization of Exchange-Correlation Functionals. *J. Chem. Phys.* **1997**, *107*, 8554−8560. (b) Grimme, S.; Ehrlich, S.; Goerigk, L. Effect of the Damping Function in Dispersion Corrected Density Functional Theory. *J. Comput. Chem.* **2011**, *32*, 1456−1465

(34) Weigend, F. R.; Ahlrichs, R. Balanced Basis Sets of Split Valence, Triple Zeta Valence and Quadruple Zeta Valence Quality for H to Rn: Design and Assessment of Accuracy. *Phys. Chem. Chem. Phys.* **2005**, *7*, 3297−3305.

(35) Zhao, Y.; Truhlar, D. G. A New Local Density Functional for Main-group Thermochemistry, Transition Metal Bonding, Thermochemical Kinetics, and Noncovalent Interactions. *J. Chem. Phys.* **2006**, *125*, 194101

(36) Marenich, A. V.; Cramer, C. J.; Truhlar, D. G. Universal Solvation Model Based on Solute Electron Density and on a Continuum Model of the Solvent Defined by the Bulk Dielectric Constant and Atomic Surface Tensions. *J. Phys. Chem. B* **2009**, *113*, 6378−6396

(37) Bryantsev, V. S.; Diallo, M. S.; Goddard, W. A., III Calculation of Solvation Free Energies of Charged Solutes Using Mixed Cluster/ Continuum Models. *J. Phys. Chem. B* **2008**, *112*, 9709−9719.

Tuning the Pyridone Scaffold within a Rhodium-NHC Platform for *gem*-Specific Alkyne Dimerization via a Ligand Assisted Proton Shuttle Mechanism

Belinda Español-Sánchez,[†] María Galiana-Cameo,[†] Asier Urriolabeitia,[‡] Victor Polo,[‡] Vincenzo Passarelli,[†] Jesús J. Pérez-Torrente,[†] Ricardo Castarlenas*[,†]